國立交通大學

光電系統研究所

碩士論文

微波退火技術應用於新穎式透明非晶態銦鎵鋅氧薄膜電晶體之研究

Study of Microwave annealing Technology on Novel Transparent Amorphous Indium Gallium Zinc Oxide Thin Film Transistors

研究生：羅婉柔　　Yuan-Jou Lo
指導教授：劉柏村 教授　　Prof. Po-Tsun Liu
林建中 教授　　Prof. Chien-Chung Lin

中華民國 一零一 年 十 月

微波退火技術應用於新穎式透明非晶態銦鎵鋅氧薄膜電晶體之研究

Study of Microwave Annealing Technology on Novel Transparent Amorphous Indium Gallium Zinc Oxide Thin Film Transistors

研究生：羅婉柔　　Yuan-Jou Lo
指導教授：劉柏村 教授　　Prof. Po-Tsun Liu
林建中 教授　　Prof. Chien-Chung Lin

國立交通大學

光電系統研究所

碩士論文

A Thesis
Submitted to Institute of Photonic System
College of Photonics
National Chiao Tung University
in partial Fulfillment of the Requirements
for the Degree of
Master
in

Photonic System

October 2012

Hsinchu, Taiwan, Republic of China

中華民國 一零一 年 十 月

微波退火技術應用於新穎式透明非晶態銦鎵鋅氧薄膜電晶體之研究

研究生: 羅婉柔　　　　　　　　指導教授: 劉柏村 教授
林建中 教授

國立交通大學

光電系統研究所

摘要

非晶態氧化半導體(Amorphous Oxide Semiconductors: AOSs) 具有高載子遷移率而且可低溫沉積、可撓曲、透明性以及均勻度佳等特點已受到廣泛的重視。目前被研究的氧化半導體有 ITO、IZO、TiO_2、ZnO、In_2O_3、Ga_2O_3、IGO、a-IGZO…等。其中以透明非晶態氧化銦鎵鋅(Amorphous InGaZnO: a-IGZO)薄膜當作主動層(Active layer)的薄膜電晶體(Thin Film Transistors: TFTs)，具有載子遷移率與可靠度比傳統氫化非晶矽薄膜電晶體(a-Si:H TFT)高、均勻性優於低溫複晶矽薄膜電晶體(Low Temperature Polycrystalline Silicon TFT: LTPS TFT) 而且可低溫製程，因此 a-IGZO 薄膜電晶體具有取代氫化非晶矽薄膜電晶體與低溫複晶矽薄膜電晶體來製作主動矩陣有機發光顯示器(Active Matrix Organic Light Emitting Display: AMOLED)的潛力。但是 a-IGZO 存在著一些本質上的缺點，例如對光以及環境中的水、氧很敏感進而影響元件的穩定性。然而，a-IGZO TFT 長時間操作的可靠度也是需要探討。本論文主要研究 a-IGZO 經由微波退火後的穩定性分析、元件長時間操作的可靠度分析與紫外光影響元件穩定性分析等三個主要方向來進行探討，以期得到改善元件穩定性的方法。從實驗結果我發現，當增加微波退火時間和能量，可以提升元件穩定性與可靠度。以這個特性，最後我提出新穎式微波退火技術以改善傳統爐管退火長時間以及高溫的特性。

Study of Microwave Annealing Technology on Novel Transparent Amorphous Indium Gallium Zinc Oxide Thin Film Transistors

Student : Yuan-Jou Lo

Advisors : Prof. Po-Tsun Liu
Prof. Chien-Chung Lin

College of Photonics & Institute of Photonic System

National Chiao Tung University, Hsinchu, Taiwan

Abstract

Amorphous oxide semiconductors (AOSs) are attracted much attention due to high mobility, low temperature deposition, flexible,transmission, and uniformity.It has been investigated of AOSs, such as ITO, IZO, TiO_2, ZnO, In_2O_3, Ga_2O_3, IGO, a-IGZO,etc. Especially,the thin film transistors (TFTs) with a-IGZO thin film as active layer perform higher mobility and better reliability than conventional hydrogenated amorphous silicon TFT (a-Si: H TFT). In addition, the uniformity of a-IGZO TFT is also superior to Low Temperature Polycrystalline Silicon TFT (LTPS TFT). Therefore, the a-IGZO TFTs have the potential to replace a-Si: H TFT and LTPS TFT forming Active Matrix Organic Light Emitting Display (AMOLED). However, a-IGZO there are some inherent defect, such as sensitive to water and oxygen in ambient and light illumination thereby affect the device stability. The device reliability under GBS also has to be considered.In this thesis, we studied the interaction between microwave annealing and furnace annealing a-IGZO thin film transistors.Time dependence threshold voltage variation reliability are investigated. Photo-reaction of a-IGZO TFT under UV-illumination is also investigated. From the experimental results, increasing microwave annealing time and power can improve the device stability and reliability under GBS. Finally we successfully investigated that microwave annealing can get better electrical characteristics, stability and reliability than furnace annealing.

誌謝

首先要感謝我的指導教授劉柏村教授為我們建立了一個資源豐富的研究環境，讓我的碩士班生涯裡受益良多！無論在求學和生活中，老師都給予了我最無私的指導與關懷。除了設備完善讓我們可以有世界級的研究成果，高水準的的師資與研究團隊可以隨時與世界頂尖研究成果爭雄，成為更全方位的人才，可以在未來為校爭光，回饋培育我們的社會。

在實驗的過程中首先要非常感謝鄧立峯與傅治翔學長，一直帶領我們學弟妹，也不時給我們關心並給予指點並有情有義的帶著我們畢業。還要感謝我的兩位夥伴王薇雅與張智翔，與我在無塵室內的量測機台共度無數時光。在漫漫長夜也有破曉時分，擁有得來不易的令人欣慰的成果時，喜悅可以彼此共享。同時也感謝實驗室中一起成長的好夥伴們揚順、光廷、震碩、立煒學長以及亦君、俊彥、沁卉等這兩年以來的互相扶持與鼓勵，陪伴我度過這每一刻研究生涯。還有豐榮、玫諍與韋勳等的加入也使實驗室注入了新的活力。一起相約打球、聚餐或出遊玩樂等無數歡樂時光也將是珍貴而不可取代的美好回憶。

最後，我要感謝我的父母家人，你們的養育之恩、栽培之情與不離不棄的陪伴，比任何言語都要深刻而有力的支持著我，讓我能夠繼續堅定地朝著理想而前進。我會用一切的努力來報答，並用這篇論文獻給我最愛的家人。

Contents

Chapter 1 Introduction

Chapter 2 Experiment Procedures

Chapter 3 Results and Discussion

Chapter 4 Experimental Results and Discussion

Figure Caption

Table Caption

Chapter 1 Introduction

1.1 General background

Display is the widely used productions. We can find a lot of applications in our daily life. Therefore, display technologies become more and more important in recent years. Display industry can be considered to start from cathode ray tubes and transfer to TFTs. In this case, we need the brief introduction about TFT-LCD. The basic structure of a TFT-LCD panel, as shown in Fig. 1-1 [1], may be thought of as two glass substrates sandwiching a layer of liquid crystal. The upper glass substrate is fitted with a color filter, while the back glass substrate has transistors fabricated on it. Furthermore, the black matrix, an opaque polymer, which is deposited on the upper glass structure, blocks the environment light to illuminate the front of TFT and incidentally avoids the incorrect color mixture by back light through color filter. [2] As shown in Fig. 1-2 [2] we can see the cross-section of TFT-LCD's subpixel. However, nothing shields the light from back illumination, so the photocurrent still takes place in LCD operation. Transistors can be classified into the depletion-mode and the enhancement-mode, based on whether drain current flows through TFT when no voltage is applied to gate electrode. For the depletion-mode TFT, when the device is on, drain current flows through the device when no gate voltage is applied. For the enhancement-mode TFT, when the device is off, only leakage current flows through the TFT without applying the gate voltage. [3]

While the TFT array's scan line was selected, charging a voltage to open the switch, the data line applied a voltage to charge the storage capacitor, which the driving signals addressed the sub-pixel and therefore the liquid crystal twisted in order to correspond the gray level that data line provided.

After the scan line was selected, charging a voltage to open the switch, the data line applied a voltage to charge the storage capacitor, which the driving signals addressed the sub-pixel and therefore the liquid crystal twisted in order to correspond the gray level that data line provided. But at the same time TFTs leak current from the data line or the storage capacitor, the gray level is not precise anymore, especially deep black level—the most sensitive to human eyes. On the other hand the contrast performance (white level brightness over black level brightness) usually depends on black level, so contrast degrades by TFT's leakage current at off-state. What is more, many drawbacks of image quality, say, flicker and vertical crosstalk, occur at the condition that TFTs having large off-current.

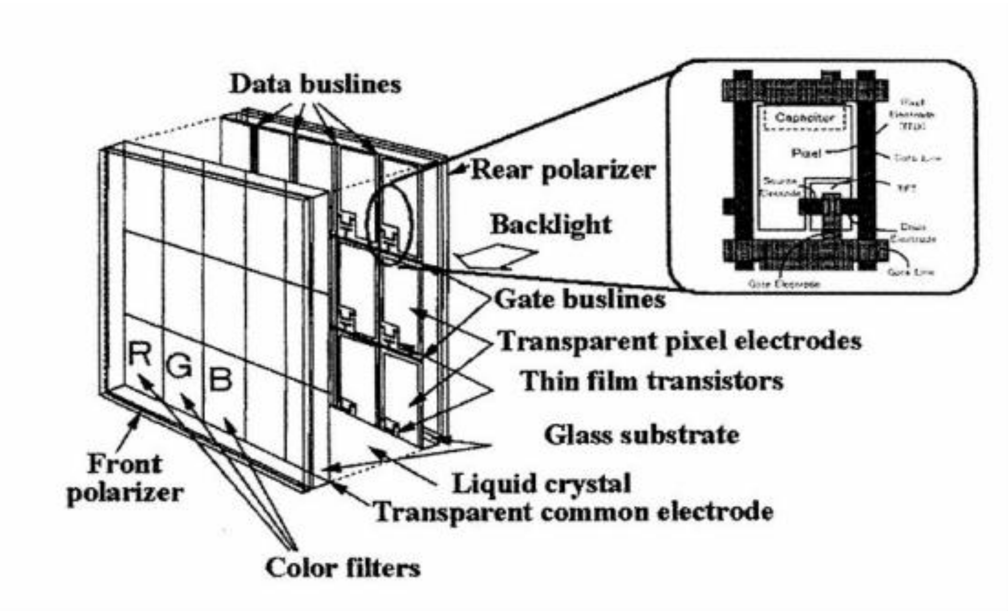

Fig. 1-1 The basic operation of the pixel array: After the scan line was selected, the data line applied a voltage to charge the storage capacitor [1]

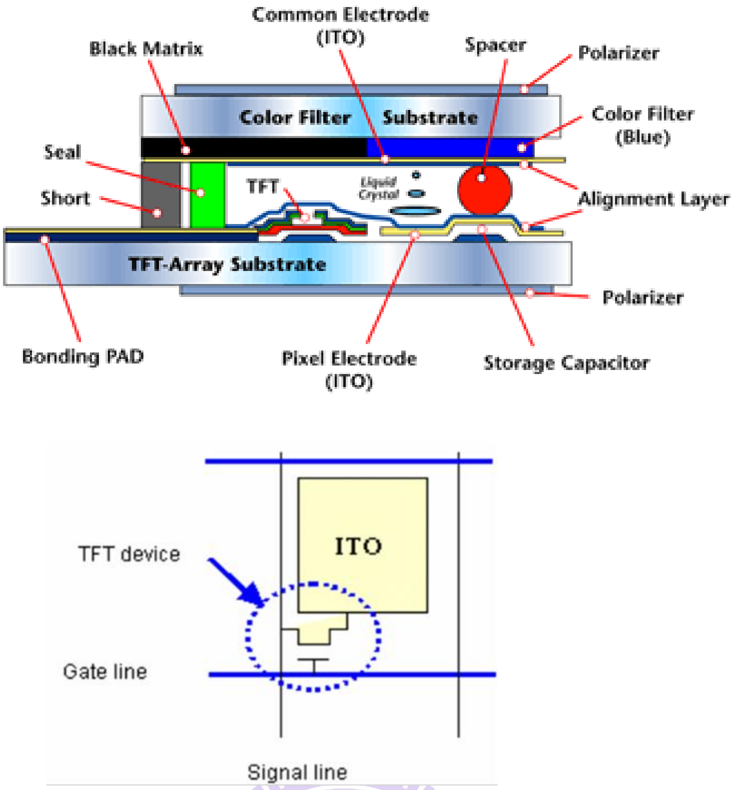

Fig. 1-2 Cross section of a LCD's subpixel [2]

Recently, a new electronics is emerging for applications because we need the performance more efficient. So far, organic molecule semiconductors have been almost exclusively examined for such applications but their performance and chemical instability are not sufficient for practical applications. According to above statements, we can find that TFTs play important roles in the flat panel display industry. For different applications, the methods of improving TFT become more and more important. In this case, we have five requirements for TFT. First, we want higher refresh rates, fast pixel switching speeds, high on/off current ratio, lower power consumption and high transmittance. [4]

1.2 Amorphous Oxide Semiconductors

1.2.1 Introduction to Amorphous Oxide Semiconductor

There're a lot of materials for TFTs' active layers. For example, we can see there are three kinds of TFT which are much wider used in flat display industry. These three are a-Si TFT, poly-Si TFT and transparent amorphous oxide semiconductor (TAOS) TFT. As we show in the Table 1-1 [5] we can see the comparison of different kind of TFTs. A-Si TFT has good stability and uniformity, but the performance isn't good enough. So it is usually choose a-Si TFT for large size display. [6] Poly-Si TFT has good stability and performance, but its uniformity isn't good enough. So it is usually choose poly-Si TFT for small size display. [6] Transparent amorphous oxide semiconductor TFT has not only good stability and uniformity but also good performance. So we chose TAOSs TFT as our active layer in this study.

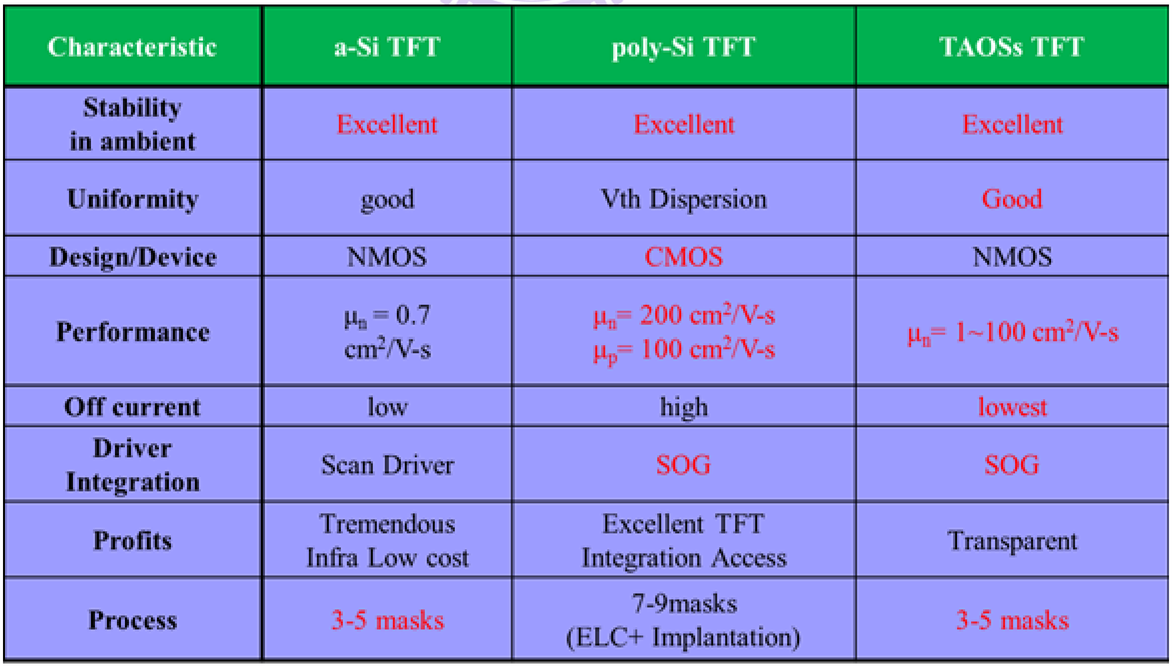

Characteristic	a-Si TFT	poly-Si TFT	TAOSs TFT
Stability in ambient	Excellent	Excellent	Excellent
Uniformity	good	Vth Dispersion	Good
Design/Device	NMOS	CMOS	NMOS
Performance	$\mu_n = 0.7$ $cm^2/V\text{-}s$	$\mu_n = 200\ cm^2/V\text{-}s$ $\mu_p = 100\ cm^2/V\text{-}s$	$\mu_n = 1\sim100\ cm^2/V\text{-}s$
Off current	low	high	lowest
Driver Integration	Scan Driver	SOG	SOG
Profits	Tremendous Infra Low cost	Excellent TFT Integration Access	Transparent
Process	3-5 masks	7-9masks (ELC+ Implantation)	3-5 masks

Table 1-1 The comparison of a-Si TFT, poly-Si TFT and TAOSs TFT [5]

According to the above statements, we can find that TAOSs TFT not only have good performance but also have other five advantages. TAOS TFT has high mobility, good uniformity and high optical transparency. It can deposit at room temperature and ease of fabrication. It also has low off current, large allowance in the choice of gate insulator and compatible with the present flat display panel industry.

Research on amorphous semiconductors started in 1950s to seek appropriate materials. The largest impact on electronics is the discovery of hydrogenated amorphous silicon (a-Si:H) by Spear and LeComber in 1975. This is the first material which can control carrier concentration by impurity doping as in crystalline and it opened a new frontier called ‘Giant Micro-electronics’ which means electronics based on circuits fabricated on a large area substrate. [7] The structure of inverted-staggered type is the most common one used in TFT-LCD products nowadays. [8] The fabrication process in TFT manufacture industry needs many thin film deposition techniques. Take the inverted-staggered bi-layer a-Si:H TFT for instance, the gate insulator (GI) and semiconductor layers can be deposited in a in-situ step (one-pump-down process). That in-situ step means “processes without breaking vacuum between two processes.” By using this “in-situ step” method, a clean interface, which is very important for high-performance device characteristics, can be easily obtained. [9] Besides, the characteristics of the interface between each layer can be easily and well controlled by only adjusting the deposition condition of each layer, such as the smoothness, composition distribution, and dangling bond passivation. The well step of fabrication can guarantee the good ohmic contact properties during the source/drain and semiconductor layer regions. In addition, the major advantages of this material are its good electronic properties such as high photoconductivity and the ability to achieve low cost fabrication at low temperatures. [10]

Transparent amorphous oxide semiconductors (TAOS) are good candidates for high performance thin film transistor devices during TFT-LCD application. It’s the materials for high performance, low processing temperature electronic devices with high mobility >> 10 $cm^2 (Vs)^{-1}$ and high transmittance about 75% in visible light portion of the electromagnetic spectrum and even when their films are deposited at room temperature. [11] However, the TAOS materials have uncontrollable carriers generated from oxygen vacancy. Therefore, it is important to design and explore a suitable material having both properties of large mobility and stable controllability of carrier concentration for practical applications.

1.2.2 The Carrier Transport Mechanism of AOSs

The mobility of a-Si:H (~1 $cm^2(Vs)^{-1}$) is much smaller than that of single crystalline Si (~200 $cm^2(Vs)^{-1}$) due to the intrinsic chemical bonding nature. The average carrier paths in covalent semiconductors, such as a-Si:H, consist of strongly directive sp^3 orbital. The bond angle fluctuation significantly alters the electronic levels, causing high density of deep tail-states, as shown in Fig. 1-3. [12]

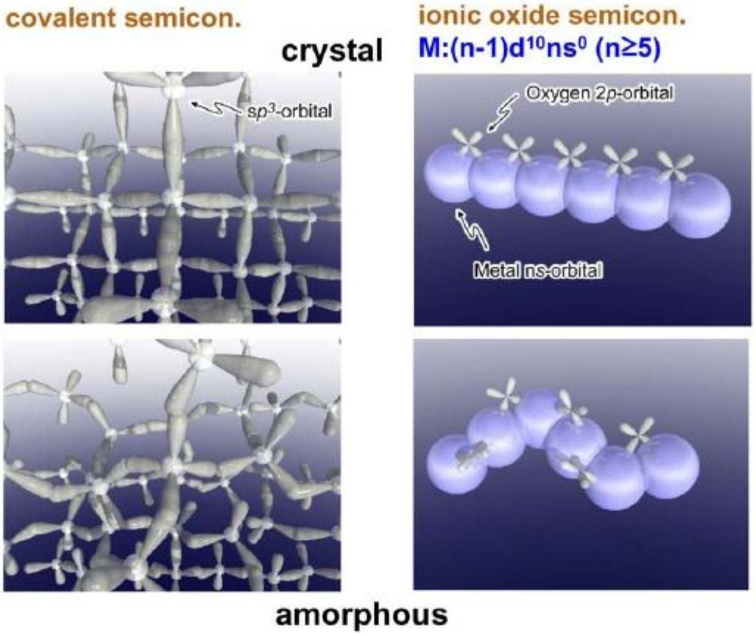

Fig. 1-3 Schematic orbital drawing of electron pathway (conduction band bottom) in conventional silicon-base semiconductor and ionic oxide semiconductor. [12]

In contrast, transport oxides constituting of heavy post transition metal cat-ions with the $(n-1)d^{10}ns^0$ electron configuration, where $n \geqq 5$, are the transparent AOS (TAOS) candidates having large mobility comparable to those of the corresponding crystals. [13] The electron pathway in oxide semiconductor is primarily composed of spatially spread ns orbital with an isotropic shape, as shown in Fig. 1-3. [13] The direct overlap among the neighboring ns orbital is possible. The degree of overlap of the ns orbital is insensitive to the distorted metal-oxygen-metal bonding. This feature shows why the Hall mobility of AOSs is similar to the corresponding crystalline phase, even under the room temperature deposition of thing-films.

1.2.3 Amorphous In-Ga-Zn-O TFTs

Among the TAOS materials, amorphous indium gallium zinc oxide (a-IGZO) is one of the most glaring candidates serving as semiconductor layer in thin film transistor (TFT). [14] However there are still many critical issues existed in a-IGZO TFT, especially for the easy absorption and desorption reaction of the oxygen atom with the surrounding atmosphere. As the oxygen species are absorbed from the ambient atmosphere, they can capture electrons in the conducting channel and form a depletion region beneath back channel layer. By following the equation of $O_{2(g)} + e^{-} \leftrightarrow O_{2}{}^{-}{}_{(s)}$, the resultant buildup of absorbed negative space charges $O_2{}^{-}{}_{(s)}$ easily repells conduction electrons and positively shifts V_{th} of a-IGZO TFT. [14] Whereas the desorption of oxygen atoms in a-IGZO back channel will result in the left shifts of V_{th}. This random reaction of absorption and desorption happening also leads to some uniformity problems. Some researching groups have applied passivation layer method to shield the back channel from the contact with ambient air. But the sequel processes would strongly affects the original properties of a-IGZO film. Therefore, the fundamental method to release the issue of environmental influence should be the improvement of the film quality of itself.

TAOSs have attracted keen attention since the high performance thin-film transistors can by obtained by using the amorphous In-Ga-Zn-O (a-IGZO) thin films for the semiconductor layers deposited on plastic substrates by using the sputter deposition at room temperature. The

TFT performance is also confirmed by using the sputter deposition [15], which demonstrates the possibility of the large-area applications. The dependence of the TFT characteristics on the metal composition is investigated in detail by a novel combinational approach, since the multi-metal AOSs can take any ratios of the composition.

The a-IGZO film has electrons as majority carriers, which is mainly affected by the oxygen vacancies and oxygen interstitials during deposition processes. [16] The ion bonding structure makes the a-IGZO TFT exhibit high field-effect carrier mobility even in the amorphous phase. [17] Even if the a-IGZO TFT owns many superior characteristics, the sensitivity to atmosphere is a extremely critical issue for the a-IGZO TFT application. [18] The environment-dependent metastability was attributed to oxygen adsorption/desorption reactions to the backchannel of the a-IGZO TFT device. The random reactions between the ambient air and the a-IGZO backchannel layer can not only change the oxygen vacancies in the a-IGZO film but result in a threshold voltage shift with days going by, and even device uniformity problems. [19] In addition to isolate the a-IGZO layer from exposing to the atmosphere, the electrical stability and uniformity of the a-IGZO film can be improved by the optimization of the chemical stoichiometry or adjusting oxygen content inherently.

For the In_2O_3-Ga_2O_3-ZnO ternary system, the incorporation of cat-ions with large ionic valance such as Ga^{3+} and Al^{3+} to high conductive oxides such as In_2O_3 and ZnO is effective to control the carrier concentration due to their strong metal-oxygen bonds. [20] Other AOSs, such as a-ITO and c-ZnO have high density carrier density, hence is difficult to control the device characteristics. Besides, amorphous In-Ga-Zn-O (a-IGZO) is transparent throughout the visible spectrum. The transmittance is greater than 80 percent from 400 nm to 850 nm as shown in Fig. 1-4. [21] Because only In^{3+} meets the electron configuration criterion $(n-1)d^{10}ns^{0}$ ($n \geqq 5$) of heavy post transition metal cat-ion for ionic AOS (IAOS) among the three cations. The mobility is primary determined by the fraction of In_2O_3 content and the highest value of ~40 $cm^{2}(Vs)^{-1}$ is obtained for the samples containing the maximum In_2O_3 fraction. The large ionic valence ions such as Ga^{3+} combine with high conductive oxides such as In_2O_3 and ZnO to control the carrier concentration effectively because of the strong metal-oxygen bonds. [22] In other words, Ga^{3+} suppresses carrier generation via oxygen vacancy formation because Ga ion forms stronger bond with oxygen than Zn and In ion. [23] Therefore, the $InGaZnO_4$ composition was chosen as the AOS for channel layer of the transparent TFT. A critical issue of semiconductor materials for TFT applications is controllability of carrier concentration.

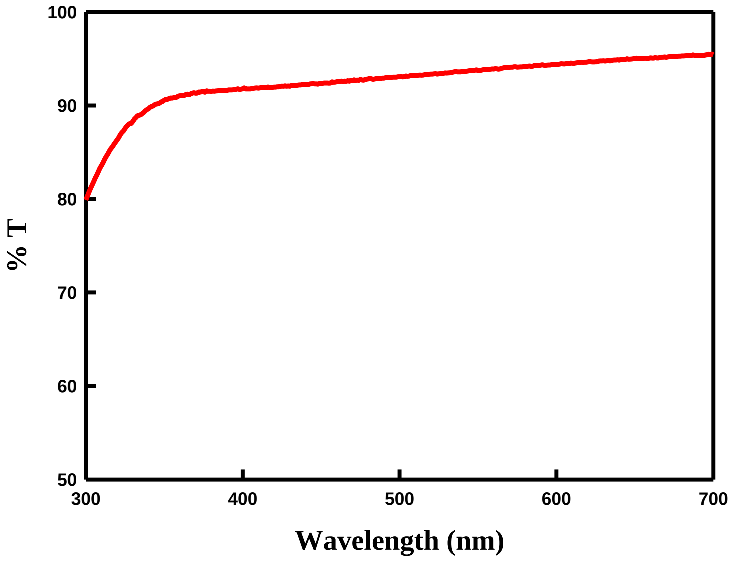

Fig. 1-4 Transmittance of a-IGZO film in visible light region. [21]

This is particularly important for AOSs because electron carriers can be easily generated. It is vital to choose materials which control carrier concentration at low levels (~10^{14} cm^{-3}) to achieve low off current (I_{off}) and large on-off current ratio (I_{on}/I_{off}). [24] In practice, the effect of binary amorphous materials in the In_2O_3-ZnO system is employed in commercial flexible transparent conductive films by depositing on plastic sheet. Thus, the effect of partial oxygen pressure was studied on the carrier concentration in a-$InGaZnO_4$ and a-$In_2Zn_3O_6$ and the results are shown in Fig. 1-5. [25] The carrier concentration in the a-$InGaZnO_4$ is distinctively reduced to below 10^{13} cm^{-3} by increasing PO_2 to 8 Pa, on the other hand, it remains at 10^{18} cm^{-3} in the a-$In_2Zn_3O_6$ deposited under the same condition. It is evident that incorporation of Ga^{3+} is supposed to attract the oxygen ions tightly due to its high ionic potential (+3 valence and small ionic radius), and thereby suppressing electron injection which is caused by oxygen ion escaping from the thin film. The Hall mobility in the samples around the chemical composition of $InGaZnO_4$ is not sensitive to the variation in the composition, as shown in Fig. 1-5. [26] Thus, the InGaZnO4 system has better electrical properties than the $In_2Zn_3O_6$ system. [27] In addition, the a-IGZO TFTs' processes are similar to that of a-Si based TFT. It means the existing production lines can be used. In this case, we can save a lot of money from buying new equipment.

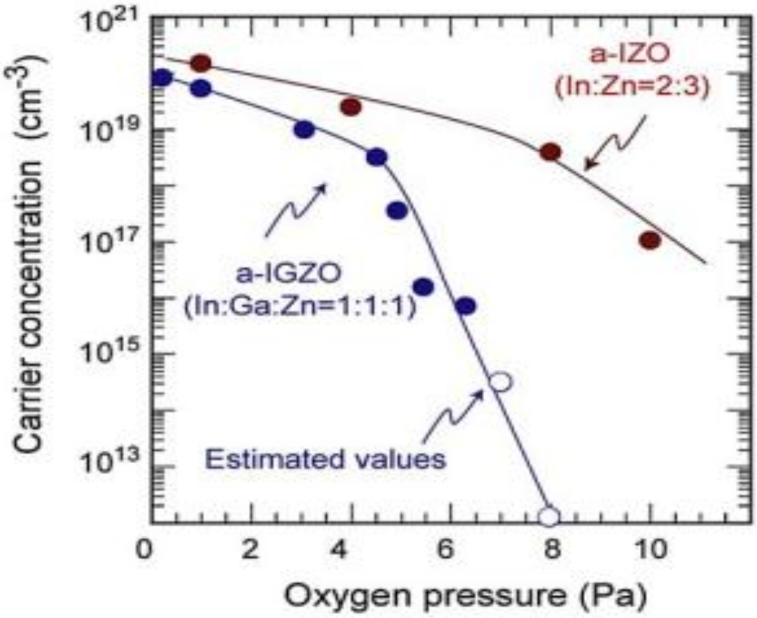

Fig. 1-5 The carrier concentration as a function of O_2 pressure during the deposition in a-$InGaZnO_4$ and a-$In_2Zn_3O_6$. [25]

1.3 Microwave Annealing

1.3.1 Interaction of Microwaves with Matter

Conventional heating usually involves the use of a furnace, which heats the walls of the furnaces by convection or conduction. The core of the sample takes much longer to achieve the target temperature. Microwave heating is able to heat the target compounds without heating the entire furnace, which saves time and energy. It is also able to heat sufficiently thin objects throughout using volumetric heating, rather than through the outer surface. Different materials convert microwave radiation to differing amounts of heat. The selectivity of different materials allows the object to be heated at differing speeds as well. [34] [38]

Microwave heating is the perspective techniques, which heat the volume of the wafer, not just its surface. It used very loosely for electromagnetic radiation in millimeter and radio frequency spectrum. Microwave processing is quite the same in thermal processing of ceramic materials. In 1990, Buchta used a microwave generator operating at 2.45GHz and a power about 1500W to heat 5-inch wafers 125mm to about 1000^{o}C over period of a few seconds. Recently Thompson and his group used a resonant chamber with a magnetron source. Dr. Bykov used a 30 GHz gyration device and a resonant processing chamber. They only demonstrated that microwave can activate at high temperature. In 2007, Jeff M. Kowalski report that microwave can activate of the heavily doped implanted layers in the range of temperature from 400-500^{o}C. [28] Microwave annealing (MWA) has a good activation situation, and can keep doped less diffusion. The conventional heating is only limited by thermal diffusivity and surface temperature. So, the deep of surface can't receive the heating energy. But microwave generate heat directly inside the exposed material as result of molecular motion. Energy is transferred throughout the entire wafer. [29] Therefore, the effective of activated is more than conventional heating. Electromagnetic (EM) radiation is a very crucial form of energy available to mankind. It consists of electric and magnetic fields that fluctuate sinusoidally in planes perpendicular to each other and propagate at the speed of light. EM radiation does not need a medium to in which to travel. [30] The dual nature of EM radiation is evident through its wave-like behavior in the case of interference and diffraction and its particle-like behavior in the case of phenomena like the photoelectric effect. The quanta of EM radiation are termed as photons. The frequency ν and the wavelength λ are inversely proportional to each other, related by $\nu = c/\lambda$, where c is the speed of light in vacuum. The energy E of the EM radiation depends linearly on the frequency ν, given by $E = h\nu$ where h is the Planck's constant. [31]

The electromagnetic spectrum is classified into regions of increasing frequencies (or equivalently, energies): radio waves, microwaves, infrared, visible light, ultraviolet, X-rays, and gamma rays. Microwaves are generally taken to have frequencies from 300 MHz to 300 GHz which correspond to wavelengths of 1 m down to 1 mm, respectively. Microwaves have found their application in diverse fields such as microwave heating, communications, RADAR, electronic warfare, radiation therapy, non-destructive testing of materials, *etc*. [32]

The interaction of microwaves with materials takes place through the two components of the microwave radiation: the electric field E and the magnetic field H. The response of a material when exposed to an electromagnetic radiation may be understood through the dielectric constant ε of the material. The dielectric constant, also known as the permittivity of the material, describes the ability of the material to be polarized in the applied electric field. To understand the dielectric response to sinusoidal fields such as the microwaves, complex permittivity ε^* is employed: $\varepsilon^* = \varepsilon' + i\,\varepsilon''$. The real part of the dielectric constant is a measure of the penetration of microwave energy in the material; while, the imaginary part indicates the ability of the material to store the energy. The dielectric properties vary with temperature and frequency. [33]

In any given material, various entities such as the free electrons, valence electrons, ions, molecular dipoles, and interfacial charges respond to the applied electric and magnetic field. The sinusoidal fields cause the charged species to polarize and vibrate. Different charged species all have different natural frequencies of vibration. The conversion to heat occurs because of the lag of the response of the material to the applied electromagnetic field. In the heating of dielectric materials, it is assumed that the magnetic field does not contribute to microwave absorption and the heating occurs entirely due to the electric field.

There are four principal polarization mechanisms in dielectric solids: [34]

a. Electronic polarization: When an atom is subjected to an external electric field, displacement of the electron cloud with respect to the nucleus gives rise to formation of a dipole. Valence electrons shift much more easily than the tightly bound core electrons. Covalent crystals have large dielectric constants owing to the displacement of the valence electrons. Thus, materials like silicon (εr’=11.9) and germanium (εr’=11.9) have high real components of the dielectric constant; hence, microwaves easily penetrate these materials.

b. Dipole polarization: Under the application of an external electric field, polar molecules orient themselves with the field. The lag associated with this response and the inter-molecular collisions lead to dielectric heating. In some materials, the polarization can be retained due to the need for thermal activation for molecular rotation, which gives rise to the formation of “electrets”.

c. Ionic or atomic polarization: Relative displacement of the positive and negative ions or atoms within molecules and crystal structures from their equilibrium lattice sites gives rise to ionic polarization.

d. Interfacial polarization: This involves the accumulation of free charges at interfaces located within the material: grain boundaries, phase boundaries and defect regions. Under the application of an electric field, the mobile charges are displaced and accumulated at such interfaces.

1.3.2 Microwave Processing of Materials

Microwaves generate rapidly changing electric fields and will generally heat any material containing mobile electric charges, such as polar molecules in a solvent or conducting ions in a solid. Polar solvents are heated as their component molecules are forced to rotate with the field and lose energy in collisions. Microwave heating a material depends to a great extent on its ‘dissipation’ factor, which is the ratio of dielectric loss or ‘loss’ factor to dielectric constant of the material. The dielectric constant is a measure of the ability of the material to retard microwave energy as it passes through; the loss factor is a measure of the ability of the material to dissipate the energy. In other words, ‘loss’ factor represents the amount of input microwave energy that is lost in the material by being dissipated as heat. [35] Therefore, a material with high loss factor is easily heated by microwave energy. In fact, ionic conduction and dipolar rotation are the two important mechanisms of microwave energy loss (i.e. energy dissipation in the material).

Microwaves are reflected from the surface and therefore do not heat metals. Metals in general have high conductivity and are classed as conductors. Conductors are often used as conduits (waveguide) for microwaves. Materials which are transparent to microwaves are classed as insulators. Insulators are often used in microwave ovens to support the material to be heated. Materials which are excellent absorbers of microwave energy are easily heated and are classed as dielectrics. [36]

Non-homogeneous material (in terms of dielectric property) may not heat uniformly, that is, some parts of the materials heat faster than others. This phenomenon is often referred to as thermal runaway. This condition can be minimized by keeping the sample in mixing or fluidized condition. Volumetric heating is the key characteristic of microwave processing. In conventional heating, the thermal energy is transferred to the material from the outside to the inside, creating a temperature gradient. Small penetration depth of infrared (less than 0.1 mm) leads to energy deposition being limited to the surface layers. [37] Microwave heating overcomes this through absorption of the microwave energy throughout the volume of the material. Since the surface loses energy by radiation, the core of the material is usually hotter and the temperature profile is the inverse of that seen in conventional heating. Volumetric heating has the advantage of uniform and rapid processing of materials leading to an increased throughput. Rapid heating in semiconductors provides the advantage of minimal diffusion of various species into the substrate.

Poorly absorbing materials (those with small values of ε”) can be hard to heat using microwaves. One common solution to this is the use of microwave susceptors to provide hybrid heating. [38] Microwave processing can also be employed for selective heating of materials, which is not possible with conventional heating.

1.4 Thesis Organization

This thesis is divided into four chapters. The main purpose of my thesis is to develop an new process method to improve the TFTs' characteristics. In my thesis, I use a-IGZO as my active layer for increasing the performance of device. Then developed new processing method: MWA for enhancing TAOS and transistor's characteristics. We will discuss the intrinsic electrical characteristics, stability and reliability in the following pages.

In chapter 1, the brief overview of flat display panel industry, operations of the TFT-LCD, the carrier transport mechanism of AOSs, amorphous In-Ga-Zn-O TFTs and microwave annealing method are introduced.

In chapter 2, the experiment procedures are introduced. The sputtering system and microwave heating system are also described. The measurement and extraction of electrical parameters are also described. The measurement of reliability on a-IGZO TFTs is described.

In chapter 3, the intrinsic electrical characteristics of a-IGZO TFTs with different MWA time and power with two kind of gate insulator (SiO_2 and SiN_x) were discussed. Then we will discuss the comparison of MWA annealing and furnace annealing. Then we will show the results of material analysis with UV-visible, X-ray diffraction, scanning electron microscope and X-ray photoelectron spectroscopy.

In chapter 4, we summarize our all experimental results and give a brief conclusion.

Chapter 2   Experiment Procedures

2.1 Experiment Procedures

Table 2.1 is the experiment flow path in my experiment. First of all, we fabricate the TFT device we want. Then we do different treatment to our device. The special part is we will do microwave annealing to our device after they are fabricated. The treatment can be classified to two ways, one is electrical analysis and the other is material analysis.

The TFT devices were chosen as a bottom-gated passivation-free inverted staggered structure and fabricated on a glass substrate. First, a 100-nm-thick Mo layer was formed as a gate electrode in a dc sputtering system and a 150-nm-thick silicon nitride (SiN_x) was subsequently deposited on the patterned gate electrode by plasma-enhanced chemical vapor deposition (PECVD). The active channel layer of a 50-nm thick IGZO layer was formed by dc sputtering with a power of 100 W at room temperature in argon (Ar) ambiance with flow rate 10 SCCM (SCCM denotes cubic centimeter per minute at STP) with target of In:Ga:Zn:O = 1:1:1:4 at.%. The sputtering was carried out at a working pressure of 3×10^{-3} torr and the base pressure was below 5×10^{-6} torr. Then, a 100-nm-thick indium tin oxide (ITO) was formed serving as source/drain electrodes by RF sputtering system and all the layers were defined by shadow mask. The channel width and length of a-IGZO TFTs were varied from 200 to 1000 μm. As we see at Fig. 2-1. Sequentially, all samples were microwave annealed at various power (1P and 2P, 1P is about 600~700 W) and time (100, 300, and 600s). 1P_100s was denoted as microwave power 600~700 W for annealing time 100s. The MWA processing time is defined as the period when the microwave power was turned on. In our experiment, the 5.8GHz microwave source has been employed for annealing process. A sample with conventional thermal annealing process was also fabricated at 450 ℃ for 1 h in a furnace with N_2 gas flow rate of 10L/hr under atmosphere pressure for comparison. All electrical and reliability measurements were carried out by using the semiconductor parameter analyzer, Keithley 4200. For the X-ray photoelectron spectroscopy measurement, X-ray diffraction, scanning electron microscope, 50-nm a-IGZO thin films with different microwave annealing conditions were deposited separately on n-type Si wafer. And measure transmittance with 50-nm a-IGZO films with different microwave annealing conditions were deposited on glass .

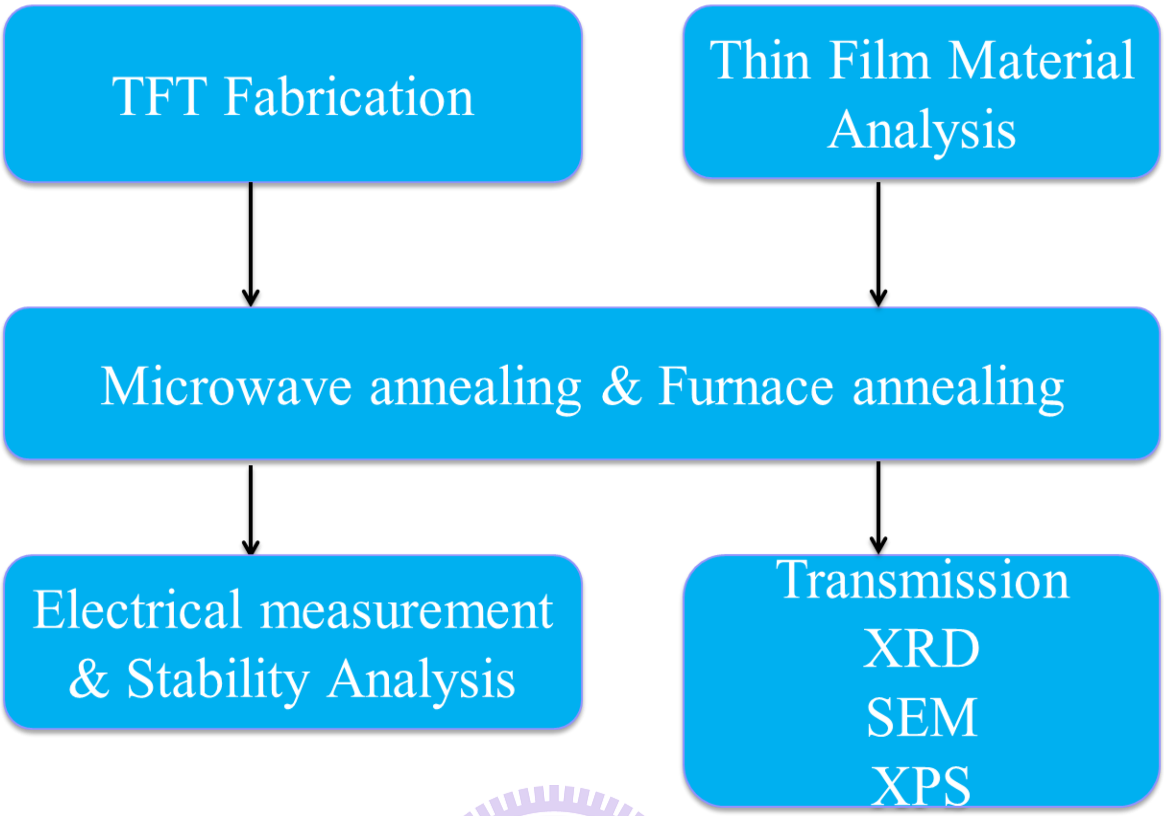

Table 2-1 Experiment flow chart

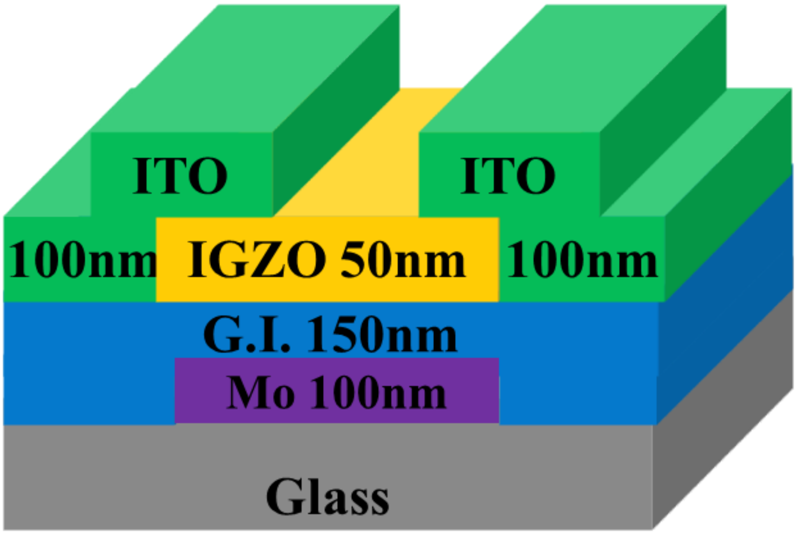

Fig. 2-1 The cross-section of a-IGZO TFTs

2.2 Sputtering systems

The experimental methods of the fabrication of the a-IGZO TFT are described. Besides, the principle of sputtering system including the RF sputtering and the DC sputtering is described. In this chapter, we will introduce two sputtering systems. One is RF sputtering and the other is DC sputtering.

RF sputtering can be applied to the deposition of both insulating conducting materials. The substrate is located above the target so that the sputtered atoms can be deposited on to the substrate. A RF power supply generates plasma at the frequency of 13.56 MHz. A RF sputtering system is shown in Fig. 2-2. [39]

DC sputtering has the advantage of higher deposition rate and is less expensive than RF sputtering. A DC sputtering is shown in Fig. 2-3 [40], the substrate is located above the target and acts as the anode. DC sputtering is commonly applied to deposit conductive materials. The plasma creates ions which are accelerated towards the target by a negative DC bias on the target. The ions bombard the target surface and dislodge the target atoms, which then deposit onto the substrate. The sputtering is performed in vacuum, typically between 1 mTorr and 50 mTorr. A lower chamber pressure increases the mean free path, which is the distance between collisions, so that the sputtered target atoms can reach the substrate without scattering away.

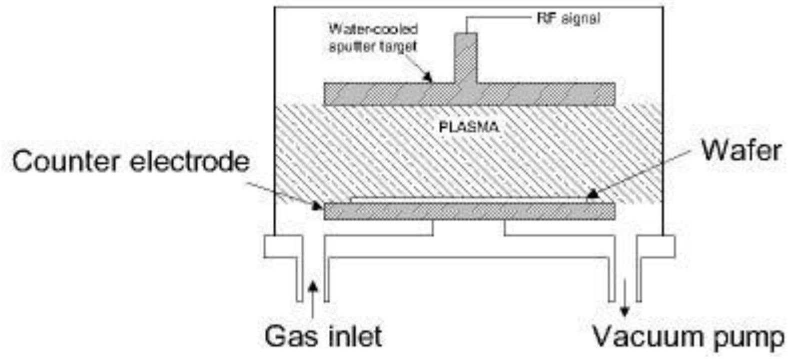

Fig. 2-2 Schematic RF sputtering system [39]

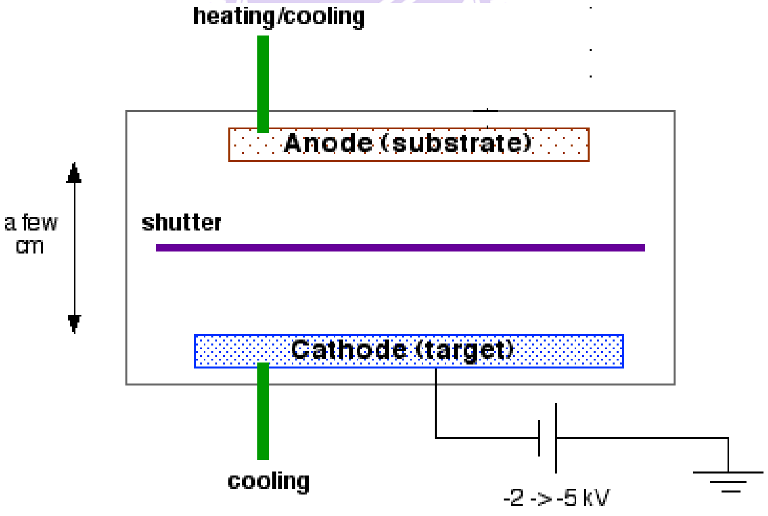

Fig. 2-3 Schematic DC sputtering system [40]

2.3 Basic Microwave Heating System

The microwave heating system is made up of four basic components: power supply, magnetron, applicator for the heating if the target material and waveguide for transporting microwaves from the generator to the applicator. Fig. 2-4(a) shows a simplistic diagram of the microwave heating system.

The microwave system mainly contains: [38]

a. Microwave power supply: supplies high voltage power for the microwave source. Supply includes internal alarms to prevent damage the microwave source, i.e. over volt alarm or over temperature alarm.

b. Microwave source: generates the microwave energy required for processing. Internal interlocks prevent overheating, i.e. water flow switch or over temperature sensor.

c. Isolator: eliminates excessive microwave energy form the process chamber to prevent damage to the microwave source.

d. Coupler: a port to measure forward microwave energy going into the process chamber.

e. Waveguide: delivers generated microwave energy into the process chamber.

f. Process chamber: an octagonal prism and vessel designed to isolate wafers from the atmosphere while gases and microwave as specified by the recipe are applied to the wafers. The chamber’s geometry promoted a uniform microwave energy field. As the Fig. 2-4 (b). [38]

When the process starts, the loading stage under the process chamber sealed. And then, the stage rotates slowly for increase the uniformity of the microwave absorption. After ten minutes N_2 gas pre-purge, the microwave power supplies turns on. The susceptors above and below the wafer can prevent particles from the environment during process. The addition of filler wafers (bare silicon) above and below the process wafer can prevent plasma generation. [39]

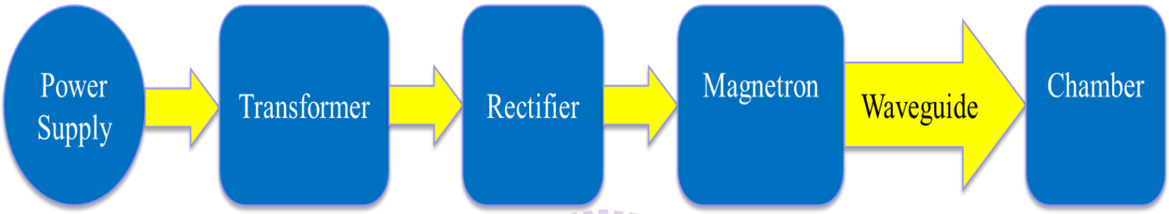

Fig. 2-4 (a) Microwave heating system.

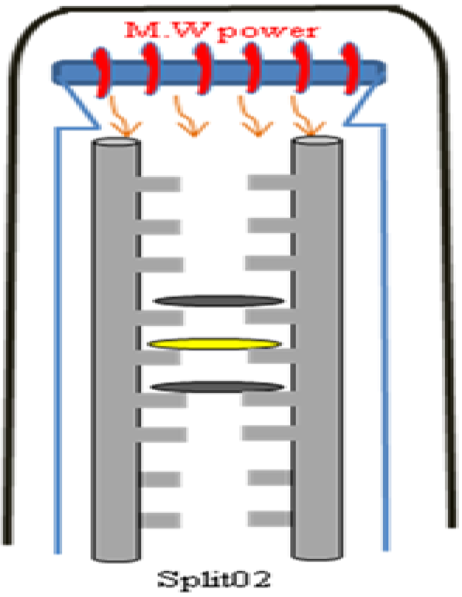

Fig. 2-4(b) The setup in the microwave chamber. The distance between adjacent slots was 1 cm only. [38]

2.4 Parameter Extraction Method

The device electrical properties were measured by a Keithley 4200 IV analyzer in a light-isolated probe station at room temperature. In I_{DS}-V_{GS} measurement, the typical drain-to-source bias was swept from V_{GS}=-20 V to V_{GS}=30 V. In this session, we describe the methods of typical parameters extraction such as threshold voltage (V_{th}), subthreshold swing (SS) and field effect mobility (μ_{FE}) from device characteristics.

Threshold voltage (V_{th}) was defined from the gate to source voltage at which carrier conduction happens in TFT channel. V_{th} is related to the gate insulator thickness and the flat band voltage. Plenty of methods are available to determine V_{th} which is one of the most important parameters of semiconductor devices. This thesis adopts the constant drain current method, which is, the voltage at a specific drain current NI_D is taken as V_{th}, that is, V_{th} = V_G (NI_D) where Vth is threshold voltage and NI_D stands for normalized drain current. Constant current method is adopted in most studies of TFTs. It provides a Vth close to that obtained by the complex linear extrapolation method. Generally, the threshold current NI_D = I_D/(W/L) is specified at 1 nA in linear region and at 10 nA in saturation region; W and L represent for TFT channel length and width, respectively. [41]

Subthreshold swing (SS, V / dec.) is a typical parameter to describe the control ability of gate toward channel which is the speed of turning the device on and off. It is defined as the amount of gate voltage required to increase and decrease drain current by one order of magnitude. SS is related to the process, and is irrelevant to device dimensions. SS can be lessened by substrate bias since it is affected by the total trap density including interfacial trap density and bulk density. In this study, SS was defined as one-half of the gate voltage required to decrease the threshold current by two orders of magnitude (from 10^{-8}A to 10^{-10}A). [41] The threshold current was specified to be the drain current when the gate voltage is equal to Vth.

Typically, μ_{FE} is determined from the transconductance (g_m) at low drain bias (V_D = 0.1 V). [41] The TFT transfer I-V characteristics can be expressed as

$$I_D = \mu_{FE} C_{ox} \frac{W}{L} [(V_G - V_{th})V_D - \frac{1}{2} {V_D}^2] \tag{2-1}$$

Where,

C_{OX} is the gate oxide capacitance per unit area,

W is channel width,

L is channel length,

V_{th} is the threshold voltage.

If V_D is much smaller than $V_G - V_{th}$ (i.e. $V_D \ll V_G - V_{th}$) and $V_G > V_{th}$, the drain current can be approximated as:

$$I_D = \mu_{FE} C_{ox} \frac{W}{L} (V_G - V_{th}) V_D \tag{2-2}$$

The g_m is defined as:

$$g_m = \mu_{FE} C_{ox} \frac{W}{L} V_D \tag{2-3}$$

Thus, $$\mu_{FE} = \frac{L}{C_{OX} W V_D} g_m \tag{2-4}$$

2.5 Measurement of reliability on a-IGZO TFTs

In this session, we will introduce two ways of reliability’s measurement. One is gate DC bias stress condition and the other is light illumination’s measurement.

The DC gate bias stress condition was set to V_G = +37.5 V for Positive Gate Bias stress (PGBS) and V_G = -37.5 V for Negative Gate Bias Stress (NGBS). Converted into electric field (E) is 2.5 MV/cm, while source and drain electrodes are connected to ground from 0s to 2000s. The sample was stressed at room temperature (25℃).

The devices was place in the dark environment (in the black box) and under room pressure and temperature. Table 2-2 shows the experiment flow of devices under light illumination. The a-IGZO TFTs with different annealing conditions were measured under different wavelength light which ranged from 900 nm (visible light) to 300 nm (UV light). The light source was a halogen optic lamp from OSRAM Inc. at 150 W generating light intensity about 63315 lx. We find the devices fabricated by the standard manufacturing processes should be placed in the box for few minutes even few hours to get stable electrical performances. And light_1_on means the specific wavelength illumination on device under measuring.

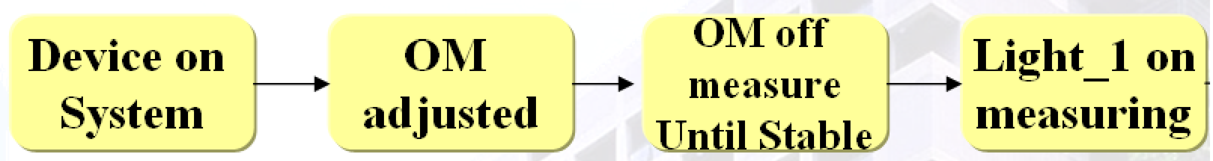

Table 2-2 The experiment flow of devices under light illumination

Chapter 3 Results and Discussion

3.1 The effect of different MWA time on a-IGZO TFT

3.1.1 a-IGZO TFT with SiO_2 gate insulator

First, we discuss the intrinsic characteristics of SiO_2 gate insulator. The drain-to-source voltage (V_{DS}) was fixed at 10 V. The gate-to-source voltage (V_{GS}) was varied from -20 V to 30 V. We fix the MWA power to 1P (600~700W) and change the MWA annealing time for 100s / 300s / 600s. Fig. 3-1 shows the results of SiO_2 gate insulator with different MWA time. We can see the line of 100s is obviously different from the other two. Table 3-1 gives us more specific results about different MWA time affect to the a-IGZO TFT with SiO_2 gate insulator. We can find that for annealing time 100s to 300s have great increases in mobility and decrease the amounts of SS / V_{th}. For the condition of MWA time 600s, we can find that it has almost the same mobility, V_{th} and SS value as the condition of MWA time 300s.

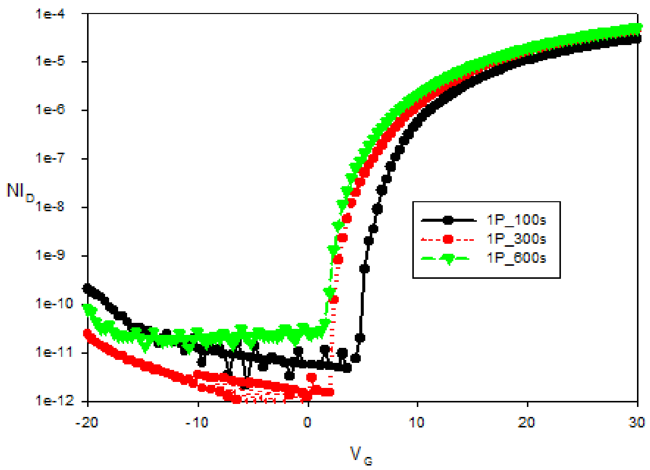

Fig. 3-1 The electrical characteristic of different MWA time for SiO_2 gate insulator

Different time	**1P_100s**	**1P_300s**	**1P_600s**
Mobility (cm^2/V-s)	3.76	5.81	5.49
Vth (V)	6.87	3.13	3.39
S.S.	0.79	0.62	0.59

Table 3-1 The data of MWA different time for SiO_2 gate insulator

Second, we will discuss the reliability of different MWA time with SiO_2 gate insulator. Fig.3-2 shows V_{th} variation of a-IGZO TFTs after being gate bias stressed with electrical field of 2.5 MV/cm for 2000s in atmosphere. V_{th} shifted in the direction of positive voltages under positive gate bias stress (PGBS). The shift amounts decrease with higher MWA time. On the other hand, we can find that negative gate bias stress (NGBS) didn't shift a lot. We find the shift amounts of V_{th} don't have obvious difference through NGBS.

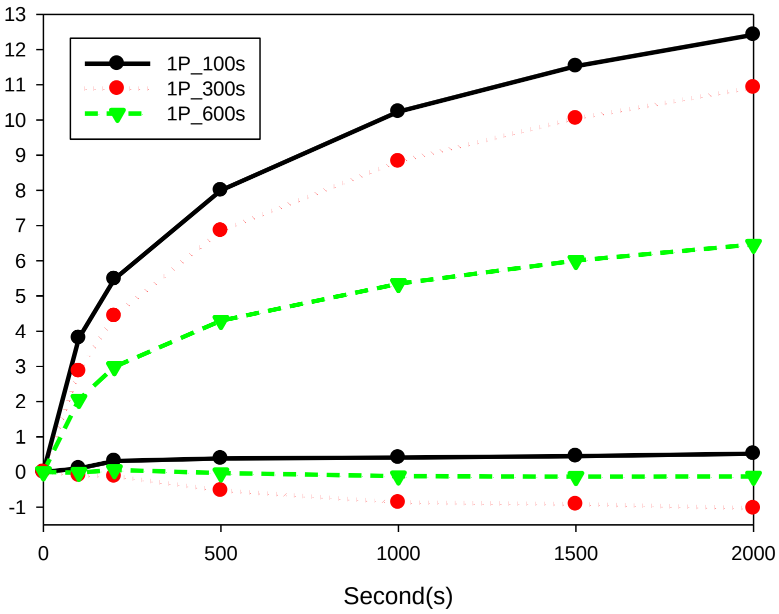

Fig. 3-2 The PBIS and NBIS results for different MWA time for SiO_2 gate insulator

3.1.2 a-IGZO TFT with SiN$_x$ gate insulator

First, we discuss the intrinsic characteristics of SiN$_x$ gate insulator. The V_{DS} was fixed at 10 V. The gate-to-source voltage (V_{GS}) was varied from -20 V to 30 V. We fixed the MWA power to 1P (600~700W) and changed the MWA annealing time for 100s / 300s / 600s. Fig. 3-3 shows the results of SiN$_x$ gate insulator with different MWA time. We can see the line of 1P_100s is obviously different from the other two. Table 3-2 gives us more specific results for different MWA time the a-IGZO TFT with SiN$_x$ gate insulator. We can find that for annealing time 100s to 600s have great increases in mobility and decrease the SS / V_{th}. For the condition of MWA time 600s, we can find it has the best results than the other two.

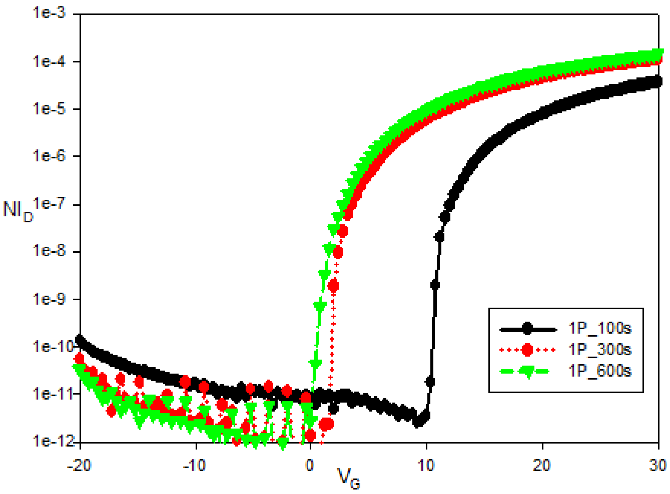

Fig. 3-3 The electrical characteristic of different MWA time for SiN$_x$ gate insulator

Different time	**1P_100s**	**1P_300s**	**1P_600s**
Mobility (cm^2/V-s)	4.86	11.51	13.40
Vth (V)	11.42	2.87	1.02
S.S.	0.55	0.57	0.30

Table 3-2 The data of different MWA time for SiN$_x$ gate insulator

Second, we will discuss the reliability of different MWA time with SiN_x gate insulator. Fig.3-4 shows V_{th} variation of a-IGZO TFTs after being gate bias stressed with electrical field of 2.5 MV/cm for 2000s in atmosphere. V_{th} shifted in the direction of positive voltages under positive gate bias stress (PGBS). The shift amounts decrease with higher MWA time. On the other hand, we can find that negative gate bias stress (NGBS) didn't shift a lot. We find the shift amounts of V_{th} don't have obvious difference through NGBS.

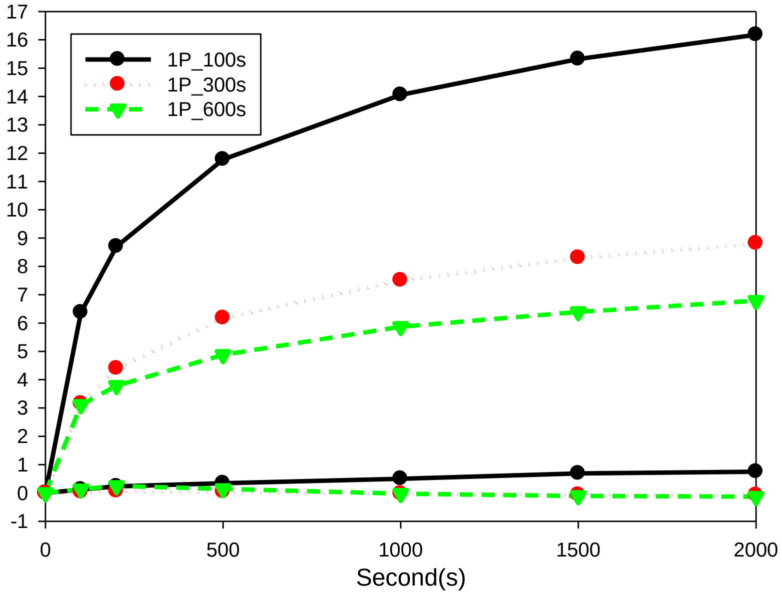

Fig. 3-4 The PBIS and NBIS results for different MWA time for SiN_x gate insulator

3.2 The effect of different MWA Power on a-IGZO TFT

3.2.1 a-IGZO TFT with SiO_2 gate insulator

First, we discuss the intrinsic characteristics of SiO_2 gate insulator. V_{DS} was fixed at 10 V. V_{GS} was varied from -20 V to 30 V. We fixed the MWA time to 100s and changed the MWA annealing time for 1P (600~700W) and 2P (1200~1400W). Fig. 3-5 shows the results of SiO_2 gate insulator with different MWA time. Table 3-3 gives us more specific results for different MWA power the a-IGZO TFT with SiO_2 gate insulator. We can find that for annealing power 1P (600~700W) to 2P (1200~1400W) have great increases in mobility and decrease the SS / V_{th}.

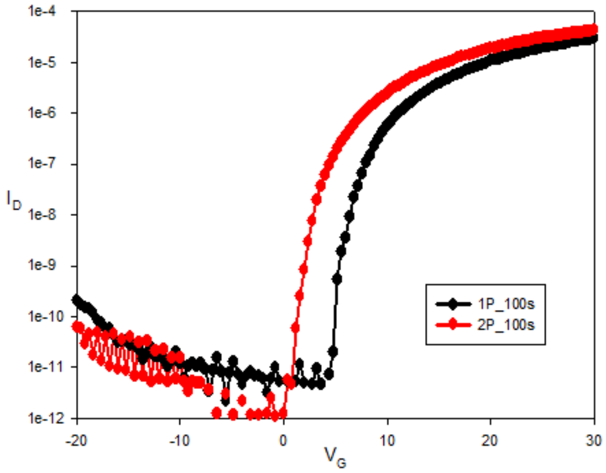

Fig. 3-5 The electrical characteristic of different MWA power for SiO_2 gate insulator

Different time	**1P_100s**	**2P_100s**
Mobility (cm^2/V-s)	3.58	4.34
Vth (V)	6.87	5.02
S.S.	0.79	0.75

Table 3-3 The data of MWA different power for SiO_2 gate insulator

Second, we will discuss the reliability of different MWA time with SiO_2 gate insulator. Fig.3-6 shows V_{th} variation of a-IGZO TFTs after being gate bias stressed with electrical field of 2.5 MV/cm for 2000s in atmosphere. V_{th} shifted in the direction of positive voltages under positive gate bias stress (PGBS). The shift amounts decrease with higher MWA power. On the other hand, we can find that negative gate bias stress (NGBS) didn't shift a lot. We find the shift amounts of V_{th} don't have obvious difference through NGBS.

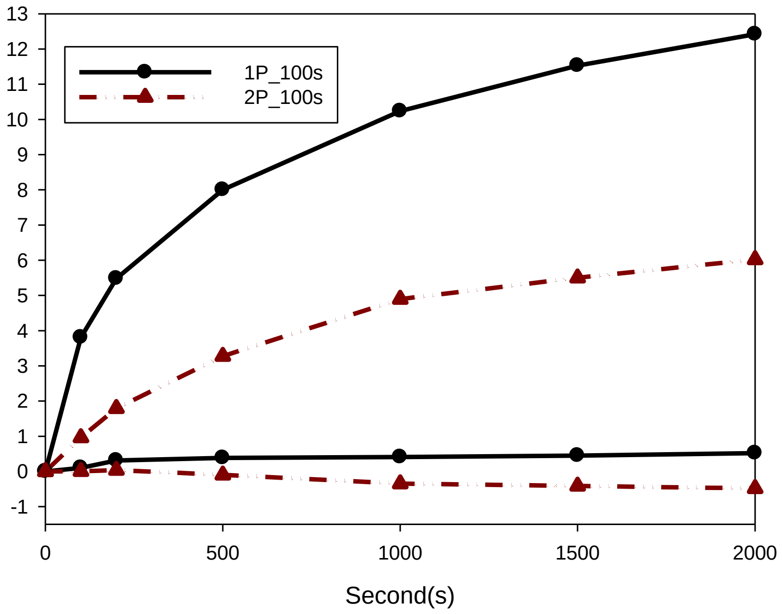

Fig. 3-6 The PBIS and NBIS results for different MWA power for SiO_2 gate insulator

3.2.2 a-IGZO TFT with SiN_x gate insulator

First, we discuss the intrinsic characteristics of SiN_x gate insulator. V_{DS} was fixed at 10 V. V_{GS} was varied from -20 V to 30 V. We fixed the MWA time to 100s and changed the MWA annealing time for 1P (600~700W) and 2P (1200~1400W). Fig. 3-7 shows the results of SiN_x gate insulator with different MWA time. Table 3-3 gives us more specific results about different MWA power the a-IGZO TFT with SiN_x gate insulator. We can find that for annealing power 1P (600~700W) and 2P (1200~1400W) has great increases in mobility and decrease the SS / V_{th}.

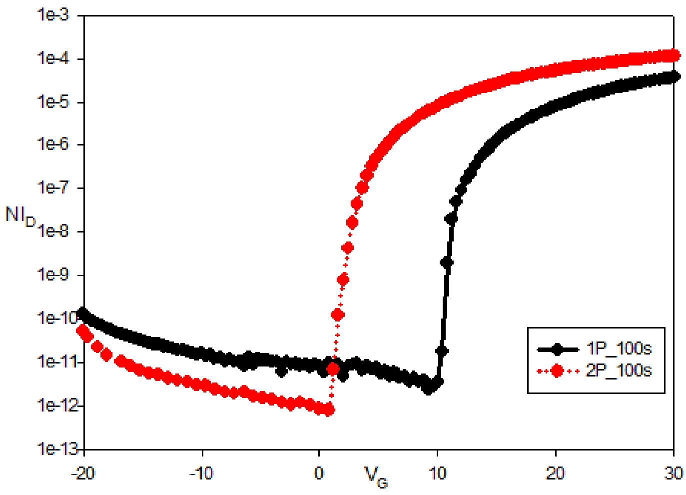

Fig. 3-7 The electrical characteristic of different MWA power for SiN_x gate insulator

Different time	1P_100s	2P_100s
Mobility (cm^2/V-s)	4.86	13.9
Vth (V)	11.42	3.12
S.S.	0.55	0.40

Table 3-4 The data of different MWA power for SiN_x gate insulator

Second, we will discuss the reliability of different MWA time with SiNx gate insulator. Fig.3-8 shows V_{th} variation of a-IGZO TFTs after being gate bias stressed with electrical field of 2.5 MV/cm for 2000s in atmosphere. V_{th} shifted in the direction of positive voltages under positive gate bias stress (PGBS). The shift amounts decrease with higher MWA time. On the other hand, we can find that negative gate bias stress (NGBS) didn't shift a lot. We find the shift amounts of V_{th} don't have obvious difference through NGBS.

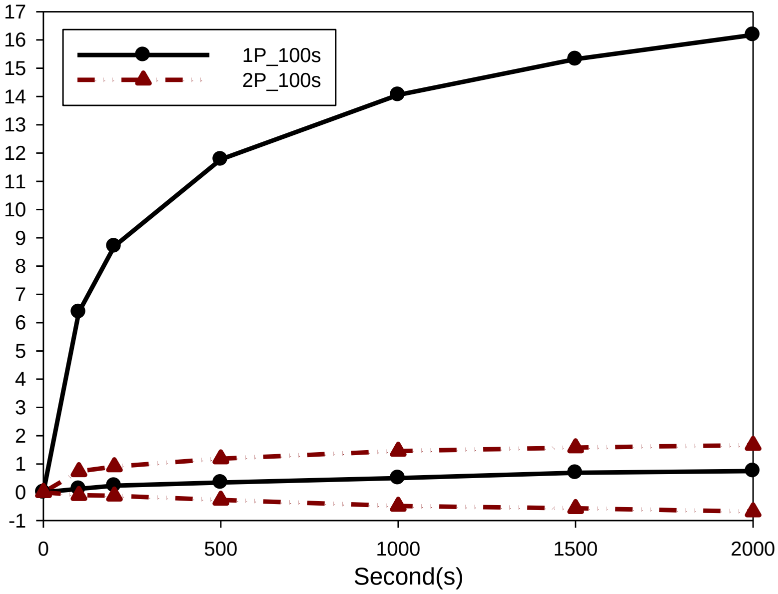

Fig. 3-8 The PBIS and NBIS results for different MWA power for SiNx gate insulator

3.3 The Comparison of MWA and Furnace Annealing on a-IGZO TFT

3.3.1 a-IGZO TFT with SiO_2 gate insulator

First, we discuss the intrinsic characteristics of SiO_2 gate insulator. V_{DS} was fixed at 10 V. V_{GS} was varied from -20 V to 30 V. We chose the best two conditions: 1P_300s and 1P_600s, comparing with furnace annealing. Fig. 3-9 shows the results of SiO_2 gate insulator with different MWA conditions and furnace annealing. Table 3-5 gives us more specific results of different MWA conditions and furnace annealing affect to the a-IGZO TFT with SiO_2 gate insulator. We can find that for the condition of MWA time 300s and 600s have the similar results, comparing with furnace annealing, we can find that MWA has great increases in mobility and decrease the SS / V_{th}.

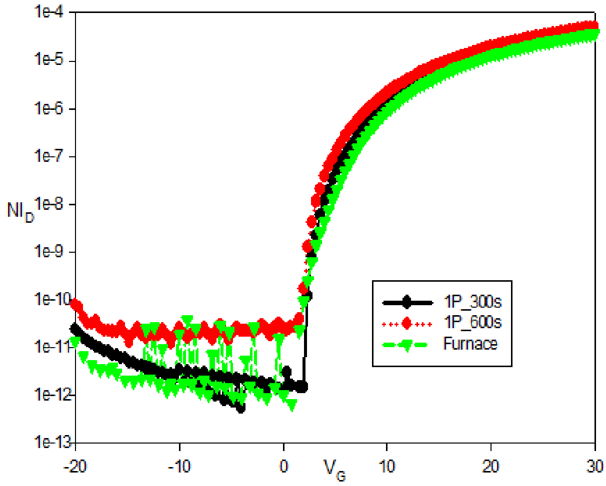

Fig. 3-9 Electrical characteristic comparison with MWA and furnace annealing for SiO_2 gate insulator

Different time	**1P_300s**	**1P_600s**	**Furnace**
Mobility ($cm^2/V\text{-}s$)	5.81	5.49	5.33
Vth (V)	3.13	3.39	3.53
S.S.	0.62	0.59	1.25

Table 3-5 The data of comparison with MWA and furnace annealing for SiO_2 gate insulator

Second, we will discuss the reliability of different MWA time with SiO_2 gate insulator. Fig.3-10 shows V_{th} variation of a-IGZO TFTs after being gate bias stressed with electrical field of 2.5 MV/cm for 2000s in atmosphere. V_{th} shifted in the direction of positive voltages under positive gate bias stress (PGBS). The shift amounts decrease with higher MWA time and almost the same as furnace annealing for the condition of MWA time 600s. On the other hand, we can find that negative gate bias stress (NGBS) didn't shift a lot. We find the shift amounts of V_{th} don't have obvious difference through NGBS.

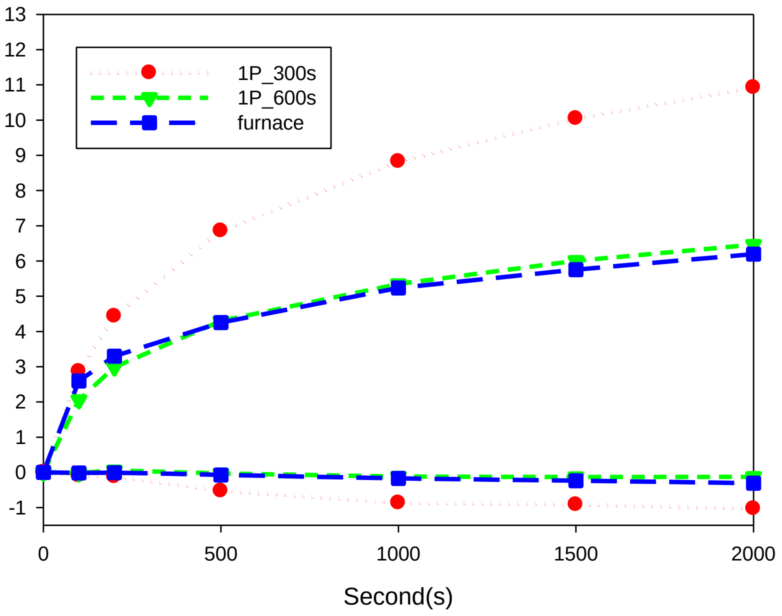

Fig. 3-10 The PBIS and NBIS comparison of MWA and furnace annealing for SiO_2 gate insulator

3.3.2 a-IGZO TFT with SiN_x gate insulator

First, we discuss the intrinsic characteristics of SiN_x gate insulator. V_{DS} was fixed at 10 V. V_{GS} was varied from -20 V to 30 V. We chose the best two conditions: 1P_ 600s and 2P_100s, comparing with furnace annealing. Fig. 3-11 shows the results of SiN_x gate insulator with different MWA conditions and furnace annealing. Table 3-6 gives us more specific results about different MWA conditions and furnace annealing affect to the a-IGZO TFT with SiN_x gate insulator. We can find that for annealing time comparing with furnace annealing, MWA condition for 1P_600s have great increases in mobility and decrease the SS / V_{th}.

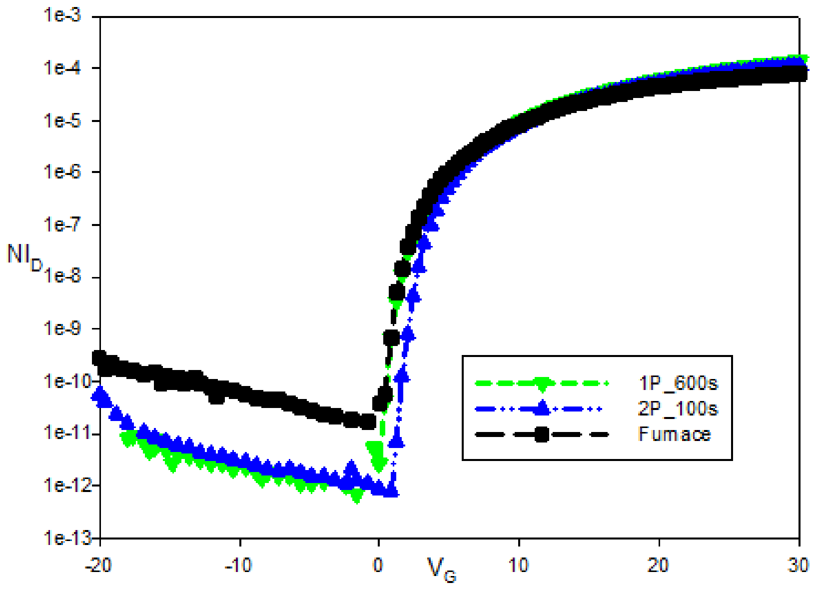

Fig. 3-11 Electrical characteristic comparison with MWA and furnace annealing for SiN_x gate insulator

Different time	**1P_600s**	**2P_100s**	**Furnace**
Mobility (cm^2/V-s)	13.40	13.9	11.7
Vth (V)	1.02	3.08	1.12
S.S.	0.30	0.40	0.41

Table 3-6 The data of comparison with MWA and furnace annealing for SiN_x gate insulator

Second, we will discuss the reliability of different MWA time with SiN_x gate insulator. Fig.3-12 shows V_{th} variation of a-IGZO TFTs after being gate bias stressed with electrical field of 2.5 MV/cm for 2000s in atmosphere. V_{th} shifted in the direction of positive voltages under positive gate bias stress (PGBS). The shift amounts decrease for MWA condition of 2P_100s and almost the same as furnace annealing. On the other hand, we can find that negative gate bias stress (NGBS) didn't shift a lot. We find the shift amounts of V_{th} don't have obvious difference through NGBS.

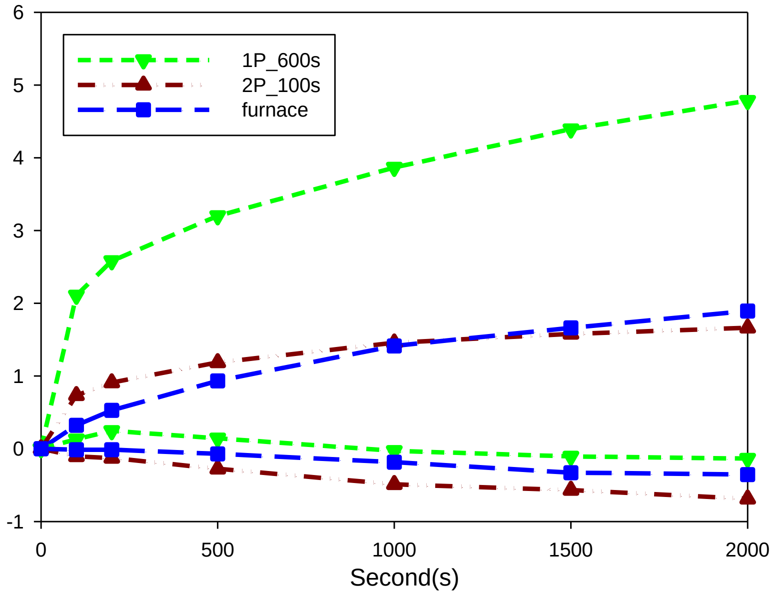

Fig. 3-12 The PBIS and NBIS comparison of MWA and furnace annealing for SiN_x gate insulator

3.4 Material Analysis Results

In this chapter, we will introduce four different material analysis results. First is UV-visible, second is X-ray diffraction, third is scanning electron microscope and the last is X-ray photoelectron spectroscopy.

First, a-IGZO TFTs with different annealing treatment were measured under different wavelength light which ranged from 900 nm (visible light) to 300 nm (UV light). The decrease of the light transmittance in UV light region can be attributed to the decrease of optical energy band-gap (E_g). The optical band-gap extract from different wavelength's transmittance of each condition was collected and compared in Table 3-7. It was clearly observed that the film didn't change their band-gap a lot from different MWA time and power. Comparing with furnace annealing, it's still not change their band-gap a lot. Which means that after post-annealing the transmittance didn't have obvious difference.

	Optical Band-gap (eV)
1P_100s	3.61
1P_300s	3.61
1P_600s	3.60
2P_100s	3.59
Furnace	3.61

Table 3-7 The data of optical band-gap for different MWA time / power and furnace annealing

Second, X-ray diffraction (XRD) is used to observe the active layer pattern shapes and prevention of hillock issues. The main diffraction peak (2θ) is 4^{o}. Range is 4^{o}~90^{o} and continue time is 1 second. Fig. 3-13 shows the results of a-IGZO TFTs with difference annealing conditions for 50nm by XRD. We can find that the XRD results for different MWA time and power didn't change films structure. Comparing with furnace annealing, MWA still remain amorphous phase. So we can find that different annealing treatment didn't change the films structure.

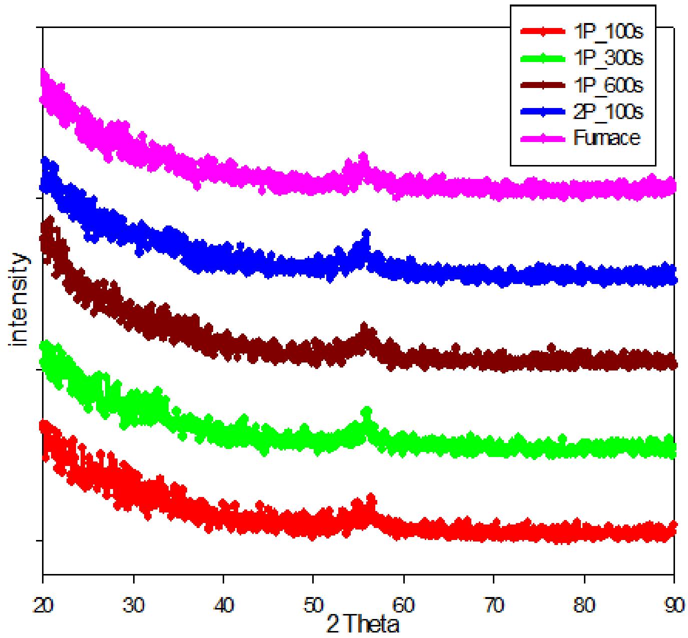

Fig. 3-13 The X-ray diffraction results for different MWA time / power and furnace annealing

Third, scanning electron microscope (SEM) images indicate the formations of films surface structure. Fig 3-14 shows the results of SEM for different annealing conditions. We can find that different MWA time and power didn't change the surface of films. Comparing with furnace, it's still have obvious difference between MWA. So we can find that different annealing conditions didn't change the surface of films.

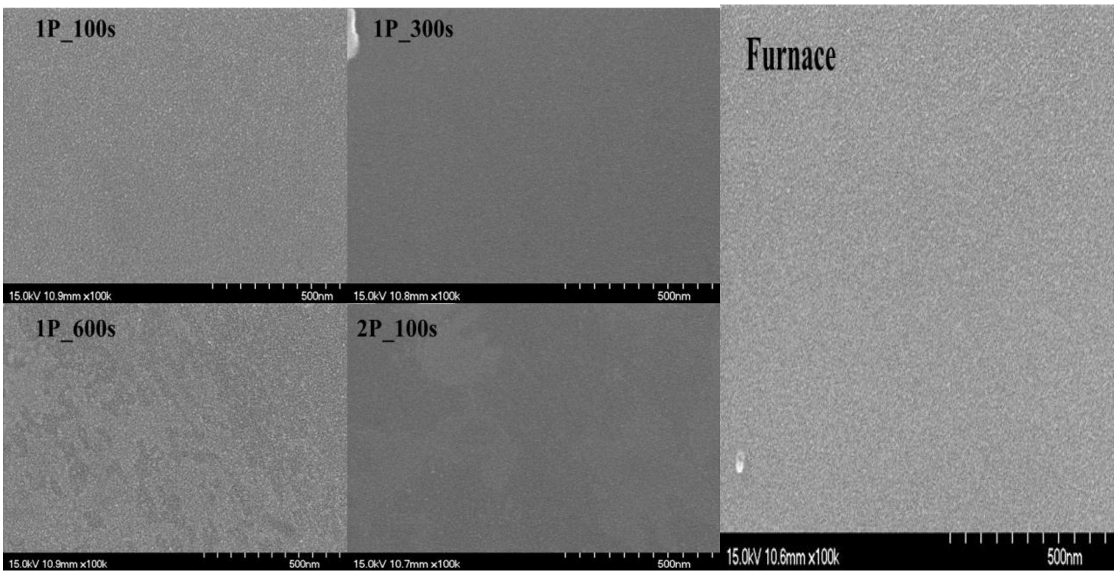

Fig. 3-14 The scanning electron microscope results for different MWA time / power and furnace annealing

The last, I will show the X-ray photoelectron spectroscopy (XPS) results. The results of XPS analysis on O1s spectrum in each a-IGZO thin film was showed in Fig. 3-15. Fig. 3-15 shows the XPS analysis results of O1s spectrum for the a-IGZO thin film with microwave annealing treatments. Two components of O1s peaks could be fitted by Gaussian Lorentzian deconvolution, which centered at 530.6 and 531.4 eV, respectively. The lower binding energy centered at 530.6 eV, denoted as peak A, originated from the lattice oxygen ions with neighboring metal atoms. [42] The higher binding energy peak at 531.4 eV, denoted as peak B, corresponds to O2_ ion at an oxygen-deficient region in the matrix of the a-IGZO film. [43] According to the results of XPS, peak A increased and peak B decreased while the microwave annealing duration increased, as shown in Fig. 3-15. Also, the XPS spectrum of a-IGZO film with high-power microwave annealing was composed of a high intensity of peak A and low intensity of peak B. This figure revealed a high content of lattice oxygen ions in the microwave-annealed a-IGZO films with few oxygen-deficient regions as the microwave power was increased. XPS analysis results confirmed that the microwave annealing process assisted the oxygen ions binding with metal atoms and suppressed the formation of oxygen-deficient region in the a-IGZO films when increasing both the microwave power and annealing duration.

Fig. 3-15(b) shows the XPS O1s spectrum of a-IGZO thin film with 2P microwave annealing for 100 s and furnace annealing at 450°C for 1 hour for comparison. The O1s peak of a-IGZO film with microwave annealing composed of a higher intensity of peak A and a lower intensity of peak B than those of the 450°C furnace-annealed one. These material analysis results were consistent with the electrical improvement in device performance and reliability of a-IGZO TFT, since microwave annealing facilitated the formation of lattice oxygen and eliminated the defects originating from oxygen deficiency. Energy transfer to the a-IGZO TFT was even more effective by the microwave annealing process than that of the conventional furnace annealing.

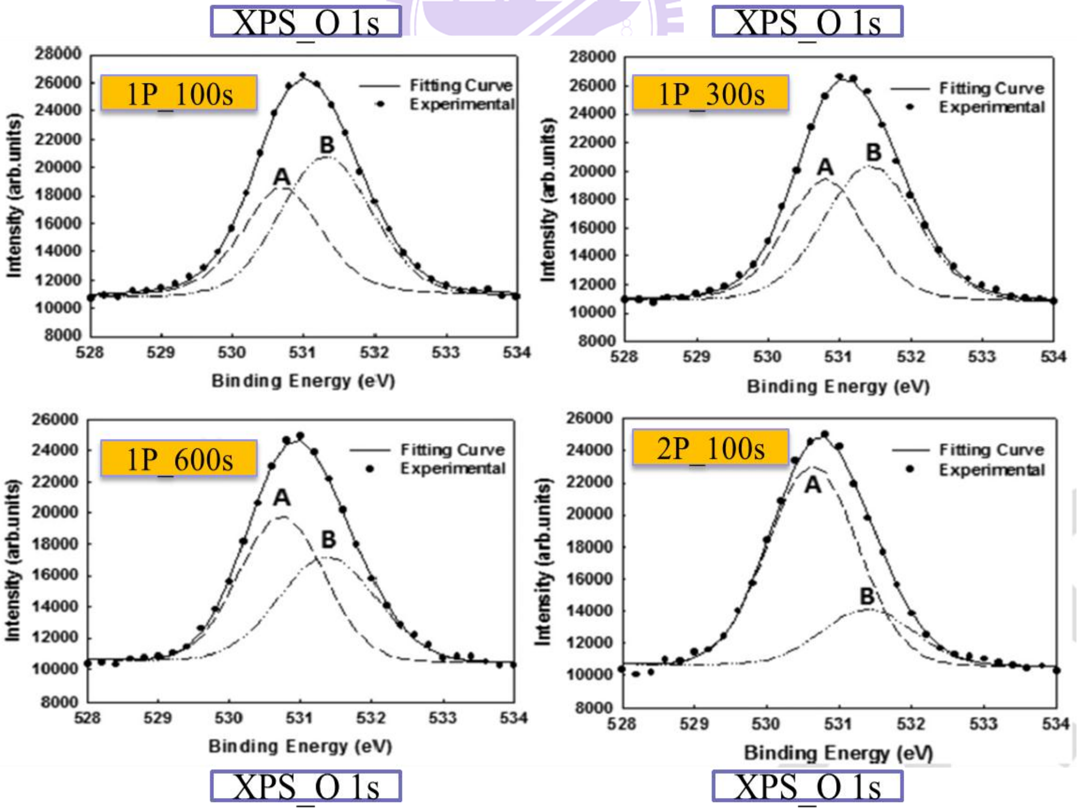

Fig. 3-15 The X-ray photoelectron spectroscopy results for different MWA time / power

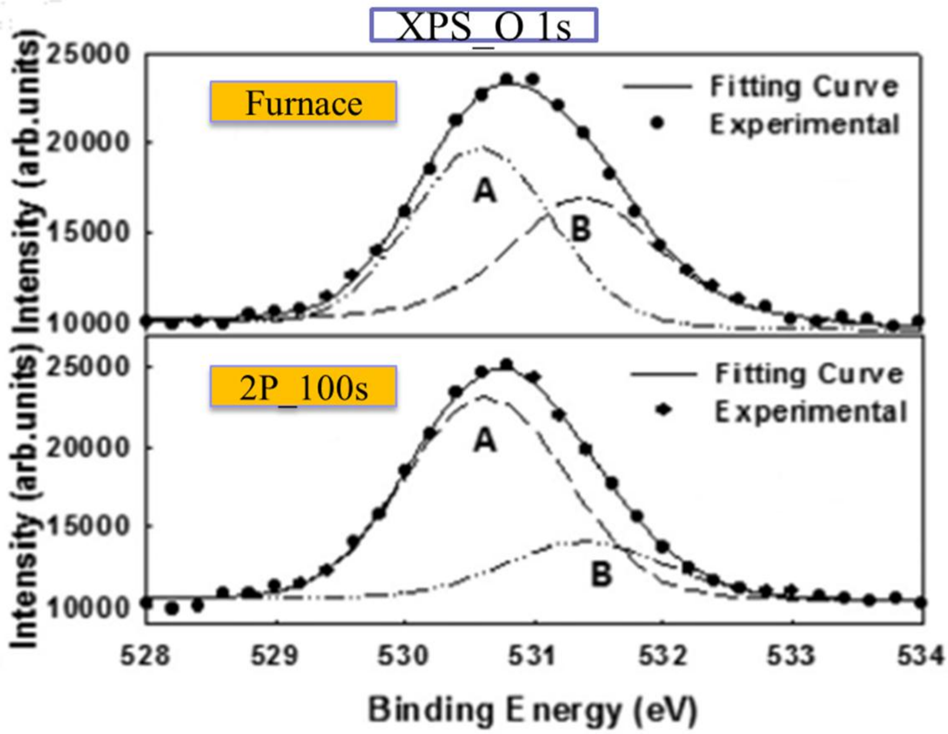

Fig. 3-16 The X-ray photoelectron spectroscopy results of 2P_100s and furnace annealing

Chapter 4 Conclusions

4.1 Conclusions

According to the statements of previous chapter, we can have the following conclusions. After 1P_300s MWA treatment, it was observed that the a-IGZO TFTs represented a lower threshold voltage (it changes from 3.53V to 3.13V), a lower sub-threshold swing (it changes from 1.25 V/dec. to 0.62 V/dec.), and a higher mobility (it changes from 5.33 cm^2/V-s to 5.81 cm^2/V-s) for SiO_2 gate insulator. After 1P_600s MWA treatment, it was observed that the a-IGZO TFTs represented a lower threshold voltage (it changes from 1.12V to 1.02V), a lower sub-threshold swing (it changes from 0.41 V/dec. to 0.30 V/dec.) and a higher mobility (it changes from 11.7 cm^2/V-s to 13.4 cm^2/V-s) for SiN_x gate insulator. The stability also get great improve by MWA. We can find that the shift amounts of V_{th} were decrease with increasing MWA time and power for both two different G.I. under the PBIS.

Through material analysis of UV-visible, XRD and SEM, we can find that the optical band-gap, phase structure, grain size and the ratio of atom composition of a-IGZO thin films were not damaged by different kind of post-treatments. But when see the results of XPS, we can find that the oxygen defects were repaired and the oxygen bonding was become stronger by increasing MWA time and power.

We can find that MWA can have the performance as good as (even better than) furnace annealing for low thermal budget and short working time. This method has great potential for applying in high-resolution display products and flexible electronics.

In summary, this work has demonstrated the feasibility of high performance and reliable a-IGZO TFTs with microwave annealing process. Microwave annealing with low thermal budget can reduce the manufacturing process period and improve electrical characteristics of a-IGZO TFTs, due to the effective absorption of microwave energy by the a-IGZO active layer. This selective heating also potentially avoided the damage to materials neighboring the a-IGZO channel layer in the TFT device structure during thermal processes. With optimum microwave annealing around 1200W for 100s in this work, electrical performance and reliability of a-IGZO TFT are more significantly promoted than with furnace annealing at 450°C for 1h. Results of this study significantly contribute to microwave annealing applications for us in emerging flat-panel displays of transparent oxide TFTs technology.

References

[1] Y. Kuo, Thin Film Transistors: Material and Process, Chap.1, p.7(2004)

[2] K. Nomura, H. Ohta, A. Takaji, T. Kamlya, M. Hirano, H. Hosono, “Room-temperature fabrication of transparent flexible thin-film transistors using amorphous oxide semiconductors”, Nature, Vol. 432, p. 488-492 (2004)

[3] K. Nomura, A. Takagi, T. Kamiya, H. Ohta, M. Hirano, and H. Hosono, “Amorphous Oxide Semiconductors for High-Performance Flexible Thin-Film Transistors”, Jpn. J. Appl. Phys., Vol. 45, p. 4303-4308 (2006)

[4] D. B. Thomason, T. N. Jackson, “High mobility tri-layer a-Si:H thin-film transistors with ultrathin active layer”, IEEE Electron Device Letters, Vol. 18, p. 397-399(1997)

[5] D. B. Thomason, T. N. Jackson, “Fully self-aligned tri-layer a-Si:H thin-film transistors with deposited doped contact layer”, IEEE Electron Device Letters, Vol. 19, p. 124-126(1998)

[6] H. Yabuta, M. Sato, K. Abe, T. Aiba, T. Den, H. Kumomi, K. Nomura, T. Kamiya and H. Hosono, “High-mobility thin-film transistor with amorphous InGaZnO4 channel fabricated by room temperature rf-magnetron sputtering”, Appl. Phys. Lett., Vol. 89, p. 2123-2125(2006)

[7] J. S. Park, J. K. Jeong, H. J. Chung, Y. G. Mo, and H. D. Kim, “Electronic transport properties of amorphous indium-gallium-zinc oxide semiconductor upon exposure to water”, Appl. Phys. Lett., Vol. 92, p. 2104-2106(2008)

[8] H. Gleskova and S. Wagner, “Amorphous silicon thin-film transistors on compliant polyimide foilsubstrates”, IEEE Electron Device Letters, Vol. 20, p. 473-475(1999)

[9] D. Kang, H. Lim, C. Kim, I. Song, and J. G. Chung, “Amorphous gallium indium zinc oxide thin film transistors: Sensitive to oxygen molecules”, Appl. Phys. Lett., Vol. 90, p. 2101-2103 (2007)

[10] S. Wagner, H. Gleskova, I. C. Cheng, M. Wu, “Silicon for thin-film transistors”, Thin Solid Film, Vol. 430, p. 15–19 (2003)

[11] S. Uchikoga, M. Kakinoki, M. Nakajima, and K. Suzuki, “A back-side passivation film on a-Si:H thin film transistor”, J. Appl. Phys. Lett., Vol. 76, p. 2484-2489 (1994)

[12] Y. Takahashi, M. Kananori, A. Kondon, “Photoconductivity of Ultrathin Zinc Oxide Films”, Jpn. J. Appl. Phys., Vol.33, p. 6611-6615(1994)

[13] J. K. Jeong, H. W. Yang, J. H. Jeong, Y.-G. Mo, and H. D. Kim, “Origin of threshold voltage instability in indium-gallium-zinc oxide thin film transistors”, Appl. Phys. Lett., Vol. 93, p. 3508-3510(2008)

[14] P. T. Liu, Y. T. Chou, L. F. Teng, and C. S. Fuh, “High-gain complementary inverter with InGaZnO/pentacene hybrid ambipolar thin film transistors”, Appl. Phys. Lett., Vol. 97, p. 3505-3507(2010)

[15] T. Kamiya, K. Nomura, and Hideo Hosono, “Electronic Structures Above Mobility Edges in Crystalline and Amorphous In-Ga-Zn-O: Percolation Conduction Examined by Analytical Model”, J. Disp. Technol., Vol. 5, p. 462-467(2009)

[16] H. Omura, H. Kumomi, K. Nomura, T. Kamiya, M. Hirano, and H. Hosono, “First-principles study of native point defects in crystalline indium gallium zinc oxide”, J. Appl. Phys., Vol. 105, p. 3712-3720(2009)

[17] N. L. Dehuff, E. S. Kettenring, D. Hong, H. Q. Chiang, J. F. Wager, R. L. Hoffman, C. H. Park, D. A. Keszler, “Transparent thin-film transistors with

zinc indium oxide channel layer", J. Appl. Phys., Vol. 97, p. 4505-4509 (2005)

[18] H.Q. Chiang, J.F. Wager, R.L. Hoffman, J. Jeong, D.A. Keszler, "High mobility transparent thin-film transistors with amorphous zinc tin oxide channel layer", Appl. Phys. Lett., Vol. 86, p. 3503-3505(2005)

[19] H. H. Hsieh, C. C. Wu, "Amorphous ZnO transparent thin-film transistors fabricated by fully lithographic and etching processes", Appl. Phys. Lett., Vol. 91, p. 3502-3504(2007)

[20] T. Hirao, M. Furuta, T. Hiramatsu, T. Matsuda and C. Li, "Bottom-Gate Zinc Oxide Thin-Film Transistors (ZnO TFTs) for AM-LCDs", IEEE Trans. Electron Devices, Vol. 55, p. 3136-3142(2008)

[21] W. Lim, Y. L. Wang, F. Ren, D. P. Norton, I. I. Kravchenko, J. M. Zavada, and S. J. Pearton, "Room-Temperature-Deposited Indium-Zinc Oxide Thin Films with Controlled Conductivity", Electrochem Solid-State Lett., Vol. 10, p. 267-269(2007)

[22] R. Martins, P. Barquinha, A. Pimentel, L. Pereira, and E. Fortunato, "Transport in high mobility amorphous wide band gap indium zinc oxide films", Phys. Stat. Sol., Vol. 202, p. 95-97(2005)

[23] K. Takechi, M. Nakata, T. Eguchi, H. Yamaguchi, and S. Kaneko, "Comparison of Ultraviolet Photo-Field Effects between Hydrogenated Amorphous Silicon and Amorphous InGaZnO4 Thin-Film Transistors", J. J. Appl. Phys., Vol. 48 p. 010203(2009)

[24] D. H. Zhang, J. Phys. D, "Fast photoresponse and the related change of crystallite barriers for ZnO films deposited by RF sputtering", Appl. Phys., Vol. 28, p. 1273(1995)

[25] H. C. Pan, M. H. Shiao, C. Y. Su, and C. N. Hsiao, "Influence of sputtering

parameter on the optical and electrical properties of zinc-doped indium oxide thin films", J. Vac. Sci. Technol., Vol. 23, p. 1187-1191(2005)

[26] Y. L. Wang, F. Ren, W. Lim, D. P. Norton, S. J. Pearton, I. I. Kravchenko, and J. M. Zavada, "Room temperature deposited indium zinc oxide thin film transistors", Appl. Phys. Lett., Vol. 90, p. 2103-2105(2007)

[27] J. S. Park, K. S. Kim, Y. G. Park, and Y. G. Mo, "Novel ZrInZnO Thin-film Transistor with Excellent Stability", Adv. Mater., Vol. 21, p. 329-333(2009)

[28] P. T. Liu, Y. T. Chou, L. F. Teng, F. H. Li, and H. P. Shieh, "Nitrogenated amorphous InGaZnO thin film transistor", Appl. Phys. Lett., Vol. 98, p. 2102-2104(2011)

[29] C. S. Fuh, S. M. Sze, P. T. Liu, L. F. Teng, and Y. T. Chou, "Role of environmental and annealing conditions on the passivation-free in-Ga–Zn–O TFT", Thin Solid Films, Vol. 520, p. 1489-1494(2011)

[30] T. F. Schulze, H. N. Beushausen, T. Hansmann, L. Korte, and B. Rech, "Accelerated interface defect removal in amorphous/crystalline silicon heterostructures using pulsed annealing and microwave heating", Appl. Phys. Lett., Vol. 95, p. 2108-2110(2009)

[31] H. L. Hortensius, A. Öztürk, P. Zeng, E. F. C. Driessen, and T. M. Klapwijk, "Microwave-induced nonequilibrium temperature in a suspended carbon nanotube", Appl. Phys. Lett., Vol. 100, p. 3112-3115(2012)

[32] Y. J. Lee, F. K. Hsueh, S. C. Huang, J. M. Kowalski, J. E. Kowalski, A. T. Y. Cheng, A. Koo, G. L. Luo, and C. Y. Wu, "Sulfur-Induced PtSi:C/Si:C Schottky Barrier Height Lowering for Realizing N-Channel FinFETs With Reduced External Resistance", IEEE Electron Device Lett., Vol. 30, p. 472-474(2009)

[33] Y. J. Chen, M. S. Cao, T. H. Wang, and Q. Wan, “Microwave absorption properties of the ZnO nanowire-polyester composites”, Appl. Phys. Lett., Vol. 84, p. 3367-3369(2004)

[34] R. F. Zhuo, L. Qiao, H. T. Feng, J. T. Chen, D. Yan, Z. G. Wu, and P. X. Yan, “Microwave absorption properties and the isotropic antenna mechanism of ZnO nanotrees”, J. Appl. Phys., Vol. 104, p. 4101-4105(2008)

[35] S. Y. Han, G. S. Herman, and C. H. Chang, “Low-Temperature, High-Performance, Solution-Processed Indium Oxide Thin-Film Transistors”, J. Am. Chem. Soc., Vol. 133, p. 5166-5169(2011)

[36] T. Jun, K. Song, Y. Jeong, K. Woo, D. Kim, C. Bae, and J. Moon, “High-performance low-temperature solution-processable ZnO thin film transistors by microwave-assisted annealing”, J. Mater. Chem., Vol. 21, p. 1102-1108(2011)

[37] X. F. Zhang, X. L. Dong, H. Huang, Y. Y. Liu, W. N. Wang, X. G. Zhu, B. Lv, J. P. Lei, and C. G. Lee, “Microwave absorption properties of the carbon-coated nickel nanocapsules”, Appl. Phys. Lett., Vol. 89, p. 3115-3117(2006)

[38] M. J. Kerr and A. Cuevas, “General parameterization of Auger recombination in crystalline silicon”, J. Appl. Phys., Vol. 91, p. 2473-2480 (2002)

[39] L. Qiao, F. S. Wen, J. Q. Wei, J. B. Wang, and F. S. Li, “Microwave permeability spectra of flake-shaped FeCuNbSiB particle composites”, J. Appl. Phys., Vol. 103, p. 3903-3907(2008)

[40] H. Plagwitz, B. Terheiden, and R. Brendel, “Staebler–Wronski-like formation of defects at the amorphous-silicon–crystalline silicon interface during illumination”, J. Appl. Phys., Vol. 103, p. 4506-4509(2008)

[41] A. N. Lagarkov and A. K. Sarychev, “Electromagnetic properties of composites containing elongated conducting inclusions”, Phys. Rev., Vol. 53, p. 6318-6336(1996)

[42] L. Olmedo, G. Chateau, C. Deleuze, and J. L. Forveille, “Microwave characterization and modelization of magnetic granular materials”, J. Appl. Phys., Vol. 73, p. 6992-6994(1993)

[43] M. Matsumoto and Y. Miyata, “Thin electromagnetic wave absorber for quasi-microwave band containing aligned thin magnetic metal particles”, IEEE Trans. Magn., Vol. 33, p. 4459-4464(1997)

Vita

姓名：羅婉柔

性別：女

出生日期：76.11.30

出生地：桃園

住址：桃園縣龍潭鄉三林村
　　　三角林 22 號

學歷：國立交通大學光電系統所
　　　國立清華大學工程與系統科學系

論文名稱：微波退火技術應用於新穎式透明非晶
　　　　　態銦鎵鋅氧薄膜電晶體之研究

Publication List

(A) Referred Journal Papers

[1] Li-Feng Teng, Po-Tsun Liu, Yuan-Jou Lo, and Yao-Jen Lee, "Effects of microwave annealing on electrical enhancement of amorphous oxide semiconductor thin film transistor", Appl. Phys. Lett., Vol. 101, p. 2901-2904(2012)

(B)Patents

[1] Po-Tsun Liu, Li-Feng Teng, Yuan-Jou Lo and Yao-Jen Lee, "Performance enhancement of metal oxide semiconductor device by microwave heating process", R.O.C. patent application.